Nucleon Resonance Structure Studies Via Exclusive KY Electroproduction at 6.6 GeV and 8.8 GeV

Experimental Support

Daniel S. Carman *(Contact Person, Spokesperson)*, Victor Mokeev *(Spokesperson)*,
Harut Avakian, Volker Burkert, Eugene Pasyuk
Jefferson Laboratory, Newport News, VA 23606, USA

Gleb Fedotov, Ralf Gothe *(Spokesperson)*, Iuliia Skorodumina
University of South Carolina, Columbia, SC 29208, USA

Bill Briscoe
The George Washington University, Washington, DC 20052, USA

Dave Ireland
University of Glasgow, Glasgow G12 8QQ, United Kingdom

Kijun Park
Old Dominion University, Norfolk, VA 23529

Brian Raue
Florida International University, Miami, FL 33199

Evgeny Golovach, Boris Ishkhanov, Evgeny Isupov
Skobeltsyn Nuclear Physics Institute, Moscow State University, 119899, Moscow, Russia

Haiyun Lu
University of Iowa, Iowa City, IA 52242

Ken Hicks
Ohio University, Athens, OH 45701

Annalisa D'Angelo, Lucilla Lanza
Universitá di Roma Tor Vergata and INFN Roma Tor Vergata, 00133 Rome, Italy

and the CLAS Collaboration

A New Experiment Run Group Proposal Submitted to Jefferson Lab PAC44

Theoretical Support

Robert G. Edwards, Michael R. Pennington, David G. Richards, Adam P. Szczepaniak†
Theory Center, Jefferson Laboratory, Newport News, VA 23606, USA
(†*Joint with Indiana University, Bloomington, IN 47405*)

Hiroyuki Kamano
KEK Theory Center, Institute of Particle and Nuclear Studies, High Energy Accelerator Research Organization, Tsukuba, Ibaraki 305-0801, Japan

Michael Döring, Igor Strakovsky, Ron Workman
The George Washington University, Washington, DC 20052, USA

T.-S. Harry Lee, Craig D. Roberts
Argonne National Laboratory, Argonne, IL 60439, USA

Jan Ryckebusch
Ghent University, B-9000 Ghent, Belgium

Elena Santopinto
INFN Sezione di Genova, 16146 Genova, Italy

César Fernández-Ramírez
Instituto de Ciencias Nucleares, Universidad Nacional Autónoma de México, A.P. 70-543, México D.F. 04510, México

clas
CEBAF Large Acceptance Spectrometer

A New Experiment Run Group Proposal Submitted to Jefferson Lab PAC44

Abstract

We propose to use the CLAS12 spectrometer to study $K^+\Lambda$ and $K^+\Sigma^0$ electroproduction from an unpolarized proton target with a longitudinally polarized electron beam at beam energies of 6.6 GeV and 8.8 GeV. The data will be analyzed to measure the differential cross sections, the separated structure functions σ_U, σ_{LT}, σ_{TT}, and $\sigma_{LT'}$, as well as the hyperon induced and beam-recoil transferred polarizations. The goal is to study the spectrum and structure of high-lying nucleon excited states (N^*). Exclusive final states will be measured, including the identification of the scattered electron, the electroproduced K^+, and the p from the hyperon decay. From these data a reaction model will be used to extract the $\gamma_v NN^*$ electromagnetic transition form factors for the most prominent N^* and Δ^* states decaying to KY in the range of invariant energy W from 1.6 GeV to 3 GeV and momentum transfer Q^2 from 2 GeV^2 to 7 GeV^2. This experiment is an essential component of a comprehensive program of exclusive electroproduction measurements with CLAS12 studying decays of N^* states to a number of different final state channels including πN, ηN, $\pi\pi N$, and KY, and serves as a lower-energy extension of E12-06-108A that was designed to study KY electroproduction at a beam energy of 11 GeV to probe N^* excitation at Q^2 up to 12 GeV^2. The main goal of the CLAS12 N^* program is to explore the evolution of the active degrees of freedom in N^* states from the regime of meson-baryon dressing at lower Q^2 to the regime of dressed quark contributions at higher Q^2 to gain unique access to the non-perturbative strong interactions between dressed quarks in excited nucleons of different quantum numbers and to explore the emergence of the meson-baryon cloud from the quark-gluon confinement regime.

Contents

1 Introduction

Intensive spectroscopy of the nucleon excitation spectrum and detailed studies of the structure of these excited states have played a pivotal role in the development of our understanding of the strong interaction. The concept of quarks that emerged through such studies led to the development of the constituent quark model [1, 2] (CQM) in the 1980s. As a result of intense experimental and theoretical efforts over the past 30 years, it is now apparent that the structure of the states in the nucleon excitation spectrum provide important information on how the strong interaction evolves from perturbative Quantum Chromodynamics (QCD) toward the non-perturbative regime where nucleon resonances (N^*) of different quantum numbers are generated from elementary quarks and gauge gluons. At the typical energy and distance scales found within the N^* states, the quark-gluon coupling is large. Therefore, we are confronted with the fact that quark-gluon confinement, hadron mass generation, and the dynamics that give rise to the N^* spectrum, cannot be understood within the framework of perturbative QCD. The need to understand QCD in this non-perturbative domain is a fundamental issue in nuclear physics, which the study of the spectrum and structure of N^* states can help to address. Such studies, in fact, represent a necessary step toward understanding how QCD in the regime of large quark-gluon couplings generates mass and how systems of confined quarks and gluons, i.e. mesons and baryons, are formed.

The studies of low-lying excited states of the nucleon using electromagnetic probes at four-momentum transfers $Q^2 < 5$ GeV^2 have revealed that the structure of these N^* states is a complex interplay between the internal core of three dressed quarks and an external meson-baryon cloud. N^* states of different quantum numbers have significantly different relative contributions from these two components, demonstrating distinctly different manifestations of the non-perturbative strong interaction in their generation. The relative contribution of the quark core increases with Q^2 in a gradual transition to a dominance of quark degrees of freedom for $Q^2 > 5$ GeV^2. This kinematics area still remains almost unexplored in exclusive reactions. Studies of the Q^2 evolution of N^* structure from low to high Q^2 offer access to the strong interaction between dressed quarks in the non-perturbative regime that is responsible for N^* formation. Mapping the Q^2 evolution of the structure of N^* states is an important aspect of the N^* program in Hall B with CLAS and CLAS12.

Electroproduction reactions $\gamma^* N \to N^* \to M + B$ provide a tool to probe the inner structure of the contributing N^* resonances through the extraction of the amplitudes for the transition between the virtual photon-nucleon initial state and the excited N^* state, i.e. the $\gamma_v NN^*$ electrocoupling amplitudes, which are directly related to the N^* structure. These electrocouplings can be represented by the so-called helicity amplitudes [3] $A_{1/2}(Q^2)$ and $A_{3/2}(Q^2)$ that describe N^* resonance electroexcitation for the two different helicity configurations of a transverse photon and a nucleon, and $S_{1/2}(Q^2)$ that describes the N^* resonance electroexcitation by longitudinal photons of zero helicity. Detailed comparisons of the theoretical predictions for these amplitudes with their experimental measurements form the basis of progress toward testing our understanding of non-perturbative QCD. The measurement of the $\gamma_v NN^*$ electrocouplings is needed in order to gain access to the dynamical momentum-dependent mass and structure of the dressed quark in the non-perturbative domain where the quark-gluon coupling is large [4], through mapping of the dressed quark mass function [5] and extractions of the quark distribution amplitudes for N^* states of different quantum numbers [6]. This is critical in exploring the nature of quark-gluon confinement and dynamical chiral symmetry breaking (DCSB) in baryons.

Figure 1 illustrates the two contributions to the $\gamma_v NN^*$ electrocouplings. In Fig. 1(b) the virtual photon interacts directly with the constituent quark, an interaction that is sensitive to the quark current and depends on the quark-mass function. However, the full meson electroproduction amplitude in Fig. 1(a) requires contributions to the $\gamma_v NN^*$ vertex from both non-resonant meson electroproduction and the hadronic scattering amplitudes as shown in Fig. 1(c). These contributions incorporate all possible intermediate meson-baryon states and all possible meson-baryon scattering processes that eventually result in the N^* formation in the intermediate state of the reaction. These two contributions have been separated from each another using, for example, a coupled-channel reaction model [7].

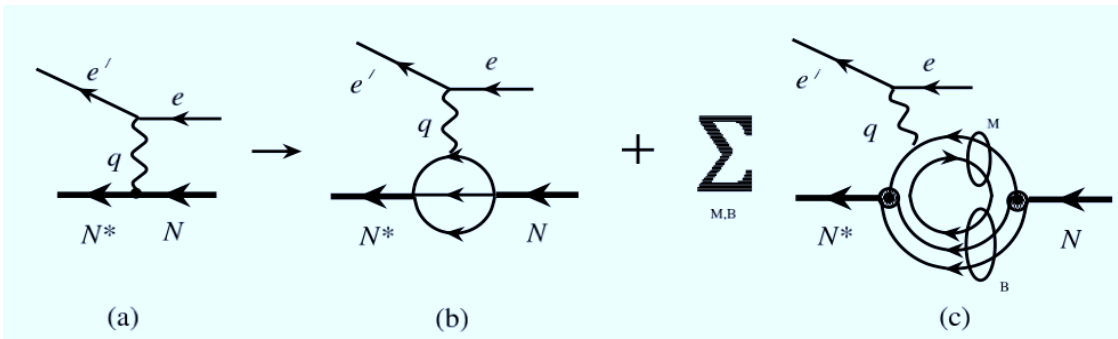

Figure 1: Schematic representation of the $\gamma^* N \to N^*$ electroproduction process [8]. (a) The fully dressed $\gamma_v NN^*$ electrocoupling that determines the N^* contribution to the resonant part of the meson electroproduction amplitude. (b) The contribution of the three-quark core. (c) The contribution from the meson-baryon cloud, where the sum is over all intermediate meson and baryon states.

Two dedicated experiments on studies of the spectrum and structure of N^* states in exclusive meson electroproduction off the proton with the CLAS12 detector have already been approved to run during the first physics running period with CLAS12. E12-09-003 [9] will measure the differential cross sections for exclusive non-strange meson (πN, ηN) and double-pion electroproduction. E12-06-108A [10] will measure differential cross sections and separated structure functions for the strangeness channels with primary focus on the $K^+\Lambda$ and $K^+\Sigma^0$ final states. These two experiments will acquire data at a beam energy of 11 GeV and probe Q^2 in the region from 5 GeV^2 to 12 GeV^2, the highest photon virtualities ever probed in these exclusive final states. From these cross section measurements, the electromagnetic transition form factors for all well-established N^* states for W up to 2 GeV to 3 GeV for 5 GeV^2 $< Q^2 <$ 12 GeV^2 will be extracted. This new proposal to study the KY final states at lower beam energies of 6.6 GeV and 8.8 GeV will allow for precision data that fully overlap the existing lower Q^2 data acquired from CLAS and the higher Q^2 data from E12-06-108A. Together these experiments will allow for measurements of precision experimental observables and structure information over an unprecedented range of Q^2 from 2 GeV^2 to 12 GeV^2.

Recent advances in the Dyson-Schwinger equations (DSE) of QCD [11, 12] have demonstrated that the external meson-baryon structure generated by confined dressed quarks in the regime of dynamical chiral symmetry breaking should be substantial. The proposed experiment will cover the transition between large distances where there are essential contributions from both the meson-baryon cloud and the quark core and small distances where the quark core is expected to dominate. Therefore the proposed experiment will address for the first time the challenging issue in hadron physics as to how the external meson-baryon cloud in the structure of N^* states is generated by the quarks and gluons confined in the inner quark core.

The invariant mass range of focus for the KY experiments, 1.6 GeV $< W <$ 3 GeV, is precisely the mass range where our knowledge of the N^* spectrum and the structure of these excited states is the most limited. While the field has slowly and methodically been making progress toward a better understanding of the low-lying N^* states in the region below 1.6 GeV, the host of the predicted missing N^* and Δ^* states lie in the region from 1.6 GeV $< W <$ 3 GeV. Figs. 2 and 3 show the N^* and Δ^* spectra predicted using the Bonn relativistically covariant quark model [13]. These figures highlight that detailed studies of the mass region provided by the KY final states will be essential to come to a more complete understanding of the structure of the states in the nucleon spectrum. Studies of the structure of the N^* states at intermediate to higher Q^2 may prove particularly valuable in this regard due to the fact that the ratio of resonant N^* to the non-resonant background contributions is expected to improve with increasing photon virtuality. As such we can hope to provide improved information on the poorly known higher-lying N^* states.

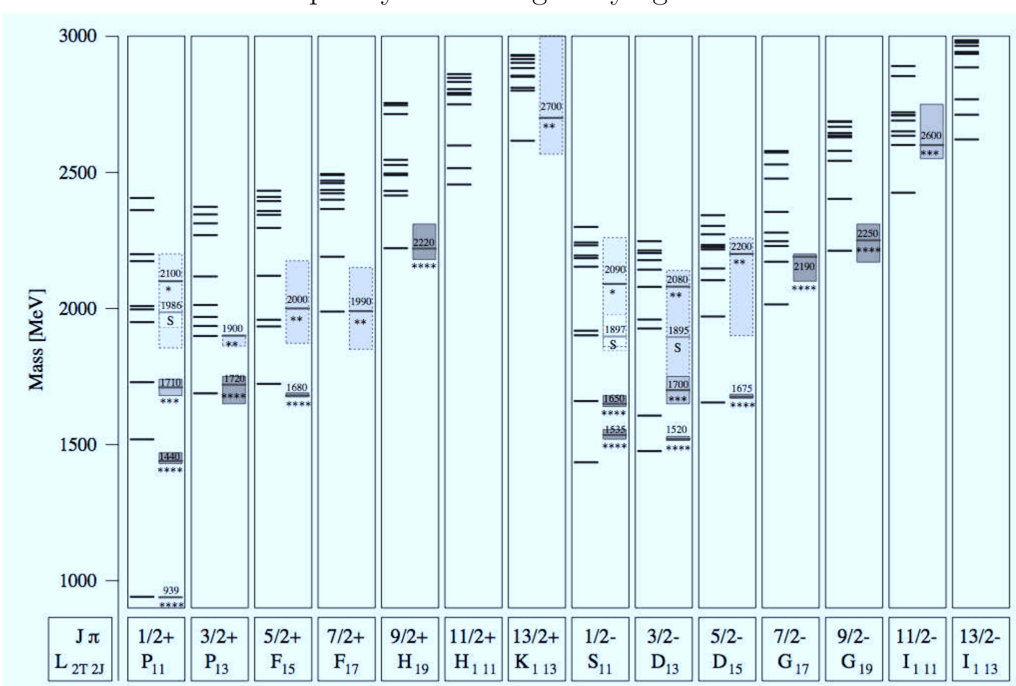

Figure 2: The calculated positive and negative parity N^* spectrum from the Bonn relativistically covariant quark model [13]. The known PDG states [14] are listed in the boxes on the right-hand side of each column.

Reliable information on KY hadronic decays from N^*s is not yet available. But the N^* electrocoupling amplitudes can be obtained from fits to the extensive existing CLAS KY electroproduction data over the range 0.5 GeV^2 $< Q^2 <$ 4 GeV^2 (see Section 2.2), which should be carried out independently in different bins of Q^2, utilizing the Q^2-independent behavior of resonance hadronic decays. The development of reaction models for the extraction

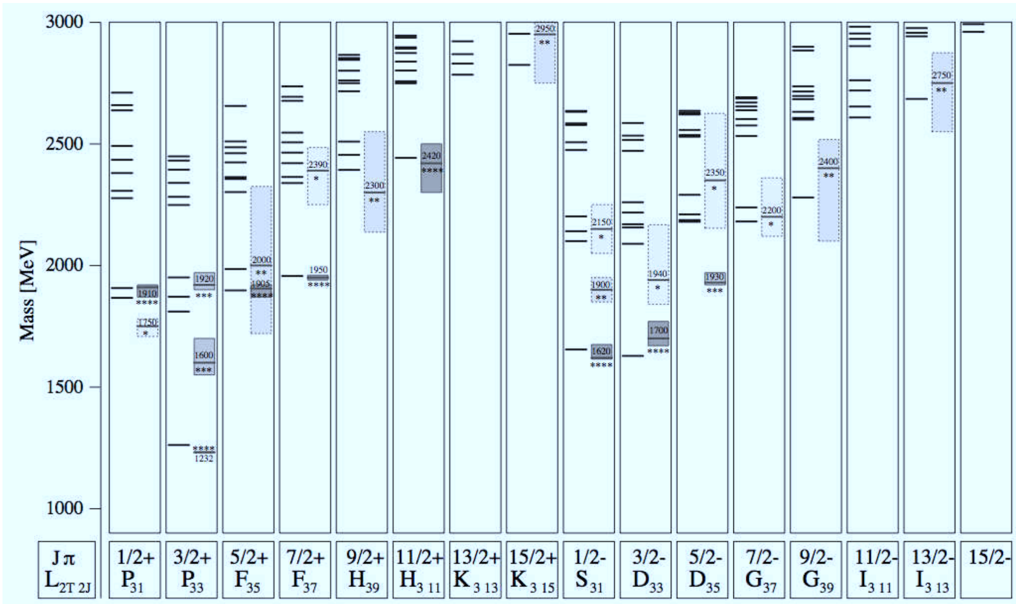

Figure 3: The calculated positive and negative parity Δ^* spectrum from the Bonn relativistically covariant quark model [13]. The known PDG states [14] are listed in the boxes on the right-hand side of each column.

of the $\gamma_v NN^*$ electrocouplings from the KY electroproduction channels is urgently needed. The work to extract the amplitudes for the prominent N^* and Δ^* states that couple to the strangeness channels $K^+\Lambda$ and $K^+\Sigma^0$ is now getting underway for the CLAS data acquired for $Q^2 < 4$ GeV^2.

Under the aegis of the existing CLAS12 N^* program (E12-09-003 and E12-06-108A), a strong collaboration between experimentalists and theorists has been brought together to achieve the challenging objectives in pursuing N^* studies from low to high Q^2 [8, 9, 10]. This new proposal to study the $N^* \to KY$ exclusive channels has been developed as an important extension of the existing CLAS12 N^* program. The main goals of this new effort are to i) provide the KY electroproduction cross sections needed for the development of the reaction models to extract the $\gamma_v NN^*$ electrocouplings that incorporate the transition from meson-baryon to quark degrees of freedom into the reaction mechanisms using the data on single-meson (including $n\pi^+$, $p\pi^0$, $p\eta$, $K^+\Lambda$, and $K^+\Sigma^0$) and double charged pion electroproduction ($p\pi^+\pi^-$) off protons for Q^2 from 2 GeV^2 to 12 GeV^2 and ii) develop approaches for the theoretical interpretation of the $\gamma_v NN^*$ electrocouplings that are capable of exploring how N^* states are generated non-perturbatively by the strong interaction in processes that emerge from QCD.

In the last decade there has been marked progress in developing more realistic and more complete theoretical approaches. CQMs have been greatly refined by using fully relativistic treatments [15, 16, 17, 18] and by including sea quark components [19], and hypercentric CQMs with more proper treatment of constituent quark interactions [20, 21] have been developed. In addition, a covariant model based on the Dyson-Schwinger equations [11, 12, 22, 23, 24] of QCD has been shown to allow the baryon data to be interpreted starting from the QCD Lagrangian.

Recently, a successful description of the data on nucleon elastic and transition $N \rightarrow \Delta(1232)\frac{3}{2}^-$ and $N \rightarrow N(1440)\frac{1}{2}^+$ form factors was achieved with the same momentum dependence of the dressed quark mass [4]. A successful description of the elastic and transition form factors for electroexcitation of N^* states of distinctly different structure conclusively demonstrated the relevance of dressed quarks as the effective degree of freedom in the structure of the ground and excited nucleons and the possibility to explore this fundamental ingredient of the non-perturbative strong interaction from the data on elastic and transition $N \rightarrow N^*$ form factors. This success emphasizes the importance of this proposed experiment as an essential part of the efforts to address the most challenging open problems of the Standard Model on the nature of >98% of hadron mass and quark-gluon confinement.

The DSE framework also provides an important link between the phenomenology of dressed current quarks and Lattice QCD (LQCD) [8]. Relations between baryon form factors and the Generalized Parton Distributions (GPDs) have also been developed that connect these two different approaches for describing baryon structure [25, 26]. On a fundamental level, LQCD is progressing rapidly toward making direct contact with the baryon data. Toward this end, the USQCD Collaboration [27] (which involves JLab's LQCD group) is working to perform calculations to predict the baryon spectrum, as well as $\gamma_v NN^*$ transition form factors.

In the past decade the Excited Baryon Analysis Center (EBAC) at JLab made significant contributions to develop rigorous approaches to not only extract the N^* parameters from the available data, but also to develop a complete framework with which to interpret these data in terms of QCD-based approaches (CQMs, DSE, LQCD). A summary of the EBAC program (completed in 2012) is detailed in Ref. [8]. Further progress is expected due to continuing developments on amplitude analysis at the JLab Physics Analysis Center [28]. Finally, the important work undertaken by the EBAC effort is being extended by the Argonne-Osaka Collaboration [7], whose goal is to extend the analysis of meson production amplitudes through their dynamical coupled-channel approach to extract the mass, width, hadronic coupling constants, and electromagnetic transition form factors of the N^* states across the full resonance region. Ultimately the results on the resonance parameters from analysis of the full set of expected meson electroproduction data from CLAS12 will allow access to the dynamics of the non-perturbative strong interaction responsible for N^* formation. These analyses will be crucial for understanding the nature of confinement and dynamical chiral symmetry breaking in baryons.

2 CLAS N^* Program

Studies of the spectrum and structure of excited nucleon states, the so-called N^* program, is one of the key cornerstones of the physics program in Hall B. The large acceptance spectrometer CLAS [29], which began data taking in 1997 and was decommissioned in 2012, was designed to measure photo- and electroproduction cross sections and polarization observables for beam energies up to 6 GeV over a broad kinematic range for a host of different exclusive reaction channels. Consistent determination of N^* properties from different exclusive channels with different couplings and non-resonant backgrounds offers model-independent support for the findings.

To date photoproduction datasets from CLAS and elsewhere have been used extensively to constrain coupled-channel fits and advanced single-channel models. However, data at Q^2=0 allows us to identify N^* states and determine their quantum numbers, but tell us very little about the structure of these states. It is the Q^2 dependence of the $\gamma_v NN^*$ electrocouplings that unravels and reveals these details. In addition, electrocoupling data are promising for studies of nucleon excited states as the ratio of resonant to non-resonant amplitudes increases with increasing Q^2. Finally, the electroproduction data are an effective tool to confirm the existence of new N^* states as the data must be described by Q^2-independent resonance masses and hadronic decay widths.

The goal of the N^* program with CLAS is to study the spectrum of N^* states and their associated structure over a broad range of distance scales through studies of the Q^2 dependence of the $\gamma_v NN^*$ electrocouplings. For each final state this goal is realized through two distinct phases. The first phase consists of the measurements of the cross sections and polarization observables in as fine a binning in the relevant kinematic variables Q^2, W, $d\tau_{hadrons}$ (where $d\tau_{hadrons}$ represents the phase space of the final state hadrons) as the data support. The second phase consists of developing advanced reaction models that describe the data over its full phase space in order to then extract the electrocoupling amplitudes for the prominent contributing N^* states.

2.1 Non-Strange Final States

Electrocoupling amplitudes for most N^* states below 1.8 GeV have been extracted for the first time from analysis of CLAS data for the exclusive π^+n and π^0p channels for Q^2 up to 5 GeV^2, for ηp for Q^2 up to 4 GeV^2, and for $\pi^+\pi^-p$ for Q^2 up to 1.5 GeV^2. Fig. 4 shows representative CLAS data for the $A_{1/2}$ electrocouplings for the $N(1440)\frac{1}{2}^+$, $N(1520)\frac{3}{2}^-$, and $N(1675)\frac{5}{2}^-$ [8, 30, 31, 32]. Studies of the electrocouplings for N^* states of different quantum numbers at lower Q^2 have revealed a very different interplay between the inner quark core and the meson-baryon cloud as a function of Q^2. Structure studies of the low-lying N^* states, e.g. $\Delta(1232)\frac{3}{2}^+$, $N(1440)\frac{1}{2}^+$, $N(1520)\frac{3}{2}^-$, and $N(1535)\frac{1}{2}^-$, have made significant progress in recent years due to the agreement of results from independent analyses of the CLAS πN and $\pi\pi N$ final states [8, 30, 32, 33, 34, 35]. The good agreement of the extracted electrocouplings from both the πN and $\pi\pi N$ exclusive channels is non-trivial in that these channels have very different mechanisms for the non-resonant backgrounds. The agreement thus provides compelling evidence for the reliability of the results.

The size of the meson-baryon dressing amplitudes are maximal for $Q^2 < 1$ GeV^2 (see Fig. 4). For increasing Q^2, there is a gradual transition to the domain where the quark degrees of freedom begin to dominate, as seen by the improved description of the N^* electrocouplings obtained within the DSE approach, which accounts only for the quark core contributions. For $Q^2 > 5$ GeV^2, the quark degrees of freedom are expected to fully dominate the N^* states [8]. Therefore, the $\gamma_v NN^*$ electrocoupling amplitudes extracted from these data at beam energies of 6.6 GeV and 8.8 GeV will probe N^* structure in the low Q^2 domain where meson-baryon degrees of freedom dominate and the high Q^2 domain where the quark core dynamics dominate.

Analysis of CLAS data for the $\pi\pi N$ channel has provided the only detailed structural information available regarding higher-lying N^* states, e.g. $\Delta(1620)\frac{1}{2}^-$, $N(1650)\frac{1}{2}^-$, $\Delta(1700)\frac{3}{2}^-$, and $N(1720)\frac{3}{2}^+$. Fig. 5 shows a representative set of illustrative examples for $S_{1/2}$

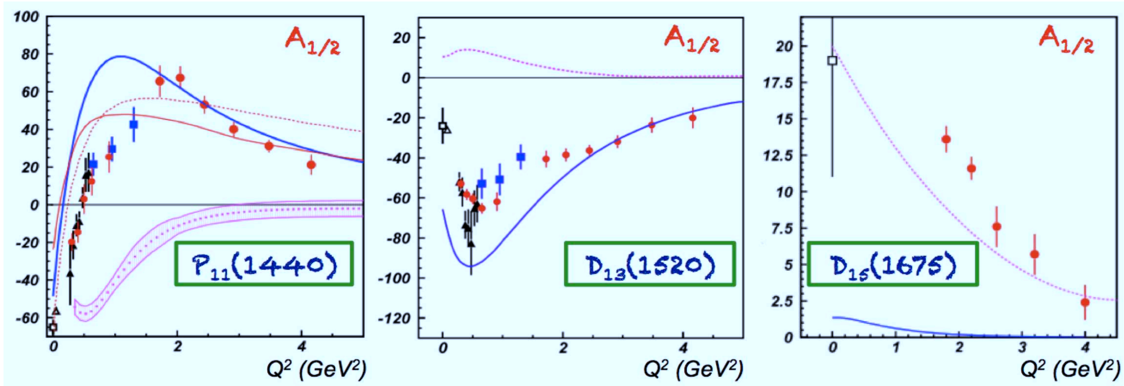

Figure 4: The $A_{1/2}$ electrocoupling amplitudes (in units of 10^{-3} GeV$^{-1/2}$) vs. Q^2 (GeV^2) for the N^* states $N(1440)\frac{1}{2}^+$ (left), $N(1520)\frac{3}{2}^-$ (middle), and $N(1675)\frac{5}{2}^-$ (right) from analyses of the CLAS πN (circles) and $\pi\pi N$ (triangles, squares) data. (Left) Calculation from a non-relativistic light-front quark model with a running quark mass (red line) and calculation of the quark core from the DSE approach (blue line). (Middle/Right) Calculations from the hypercentral constituent quark model (blue lines). The magnitude of the meson-baryon cloud contributions is shown by the magenta line (or band) on each plot. See Refs. [8, 30, 32, 31] for details on the data and the models.

for the $\Delta(1620)\frac{1}{2}^-$ [32], as well as for $A_{1/2}$ for the $\Delta(1700)\frac{3}{2}^-$ and $A_{3/2}$ for the $N(1720)\frac{3}{2}^+$ [31]. Here the analysis for each N^* state was carried out independently in different bins of W across the width of the resonance for Q^2 up to 1.5 GeV^2 with very good correspondence within each Q^2 bin. Note that most of the N^* states with masses above 1.6 GeV decay preferentially through the $\pi\pi N$ channel instead of the πN channel.

2.2 KY Final States

With a goal to have an independent determination of the electrocouplings for each N^* state from multiple exclusive reaction channels, a natural avenue to investigate the higher-lying N^* states is the strangeness channels $K^+\Lambda$ and $K^+\Sigma^0$. In fact, data from the KY channels are critical to provide an independent extraction of the electrocoupling amplitudes for the higher-lying N^* states. The CLAS program has yielded by far the most extensive measurements of KY electroproduction data ever measured across the nucleon resonance region. These measurements have included the differential cross sections and the separated structure functions σ_T, σ_L, $\sigma_U = \sigma_T + \epsilon\sigma_L$, σ_{LT}, σ_{TT}, and $\sigma_{LT'}$ for $K^+\Lambda$ and $K^+\Sigma^0$ [36, 37, 38, 39], the recoil polarization for $K^+\Lambda$ [40], and the beam-recoil transferred polarization for $K^+\Lambda$ and $K^+\Sigma^0$ [41, 42]. These measurements span Q^2 from 0.5 GeV^2 to 4.5 GeV^2, W from 1.6 GeV to 3.0 GeV, and the full center-of-mass angular range of the K^+.

The KY final states, due to the creation of an $s\bar{s}$ quark pair in the intermediate state, are naturally sensitive to coupling to higher-lying s-channel resonance states at $W > 1.6$ GeV, a region where our knowledge of the N^* spectrum is the most limited. Note also that although the two ground-state hyperons have the same valence quark structure (uds), they differ in isospin, such that intermediate N^* resonances can decay strongly to $K^+\Lambda$ final states, but intermediate Δ^* states cannot. Because $K^+\Sigma^0$ final states can have contributions from both N^* and Δ^* states, the hyperon final state selection constitutes an isospin filter. Shown

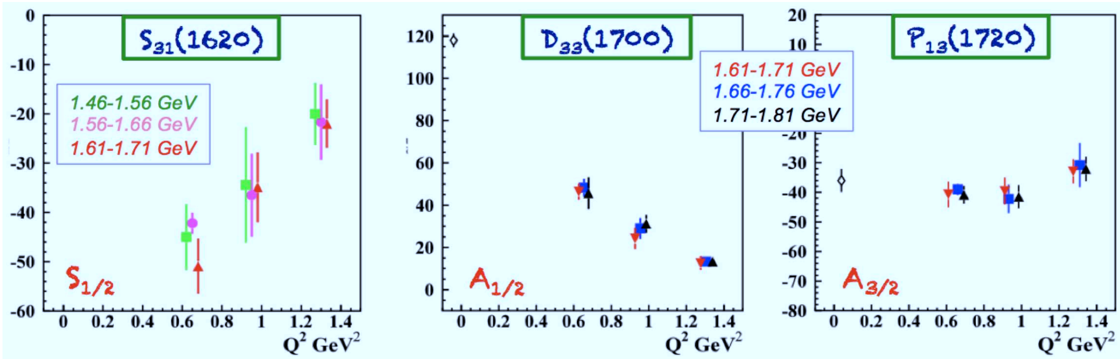

Figure 5: CLAS results for the N^* electrocoupling amplitudes (in units of 10^{-3} GeV$^{-1/2}$) from analysis of the exclusive $\pi^+\pi^-p$ final state as a function of Q^2 (GeV^2). (Left) $S_{1/2}$ of the $\Delta(1620)\frac{1}{2}^-$ [32], (middle) preliminary extraction of $A_{1/2}$ for the $\Delta(1700)\frac{3}{2}^-$ [31], and (right) preliminary extraction of $A_{3/2}$ for the $N(1720)\frac{3}{2}^+$ [31]. Each electrocoupling amplitude was extracted in independent fits in different bins of W across the resonance peak width as shown for each Q^2 bin (with the points at each Q^2 offset for clarity).

in Figs. 6 and 7 is a small sample of the available data in the form of the $K^+\Lambda$ and $K^+\Sigma^0$ structure functions σ_U, σ_{LT}, σ_{TT}, and $\sigma_{LT'}$ [39, 43], illustrating the broad kinematic coverage and statistical precision of the data.

Figures 6 and 7 include two of the more advanced single channel reaction models for the electromagnetic production of KY final states. The MX model is the isobar model from Maxwell [44], and the RPR-2007 [46] and RPR-2011 [45] models are from the Ghent Regge plus Resonance (RPR) framework. Both the MX and RPR models were developed based on fits to the extensive and precise photoproduction data from CLAS and elsewhere and describe those data reasonably well. However, they fail to adequately describe the electroproduction data in any of the kinematic phase space. Reliable information on KY hadronic decays from N^*s is not yet available due to the lack of an adequate reaction model. However, after such a model is developed, the N^* electrocoupling amplitudes for states that couple to KY can be obtained from fits to the extensive existing CLAS KY electroproduction data over the range 0.5 GeV$^2 < Q^2 <$ 4.5 GeV^2, which should be carried out independently in different bins of Q^2 with the same KY hadronic decays, extending the available information on these N^* states and testing the consistency of the analysis. The development of such reaction models for the extraction of the $\gamma_v NN^*$ electrocouplings from the KY electroproduction channels has been initiated. A key element to the development of the reaction models for $K^+\Lambda$ and $K^+\Sigma^0$ production is the inclusion of constraints provided by the hyperon polarization observables. Fig. 8 shows the $K^+\Lambda$ induced polarization data from CLAS [40] and Fig. 9 shows the $K^+\Lambda$ beam-recoil transferred polarization data from CLAS. These data are overlaid with the predictions from the MX [44] and RPR [46, 45] models and show that they provide important constraints for the resonant and non-resonant diagrams in the models even with their relatively modest statistical precision.

To date the PDG [14] lists only four N^* states, $N(1650)\frac{1}{2}^-$, $N(1710)\frac{1}{2}^+$, $N(1720)\frac{3}{2}^+$, and $N(1900)\frac{3}{2}^+$, with known couplings to $K\Lambda$ and no N^* states are listed that couple to $K\Sigma$; only a single Δ^* state, $\Delta(1920)\frac{3}{2}^+$, is listed with coupling strength to $K\Sigma$. The branching ratios to

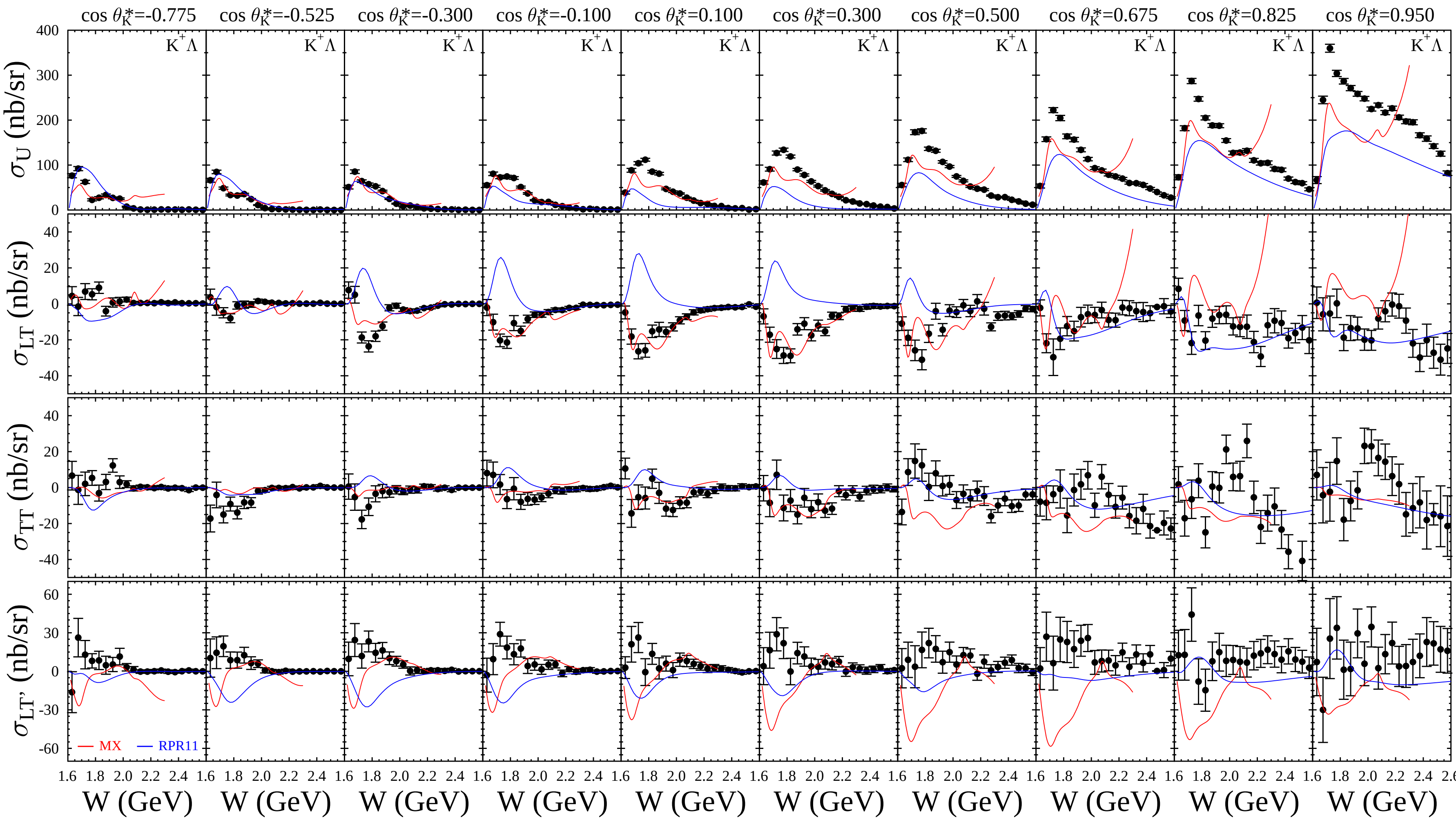

Figure 6: Structure functions $\sigma_U = \sigma_T + \epsilon\sigma_L$, σ_{LT}, σ_{TT}, and $\sigma_{LT'}$ (nb/sr) for $K^+\Lambda$ production vs. W (GeV) for E_b=5.5 GeV for Q^2=1.80 GeV^2 and $\cos\theta_K^*$ values as shown from CLAS data [39, 43]. The error bars represent the statistical uncertainties only. The red curves are from the hadrodynamic KY model of Maxwell [44] and the blue curves are from the hybrid RPR-2011 KY model from Ghent [45].

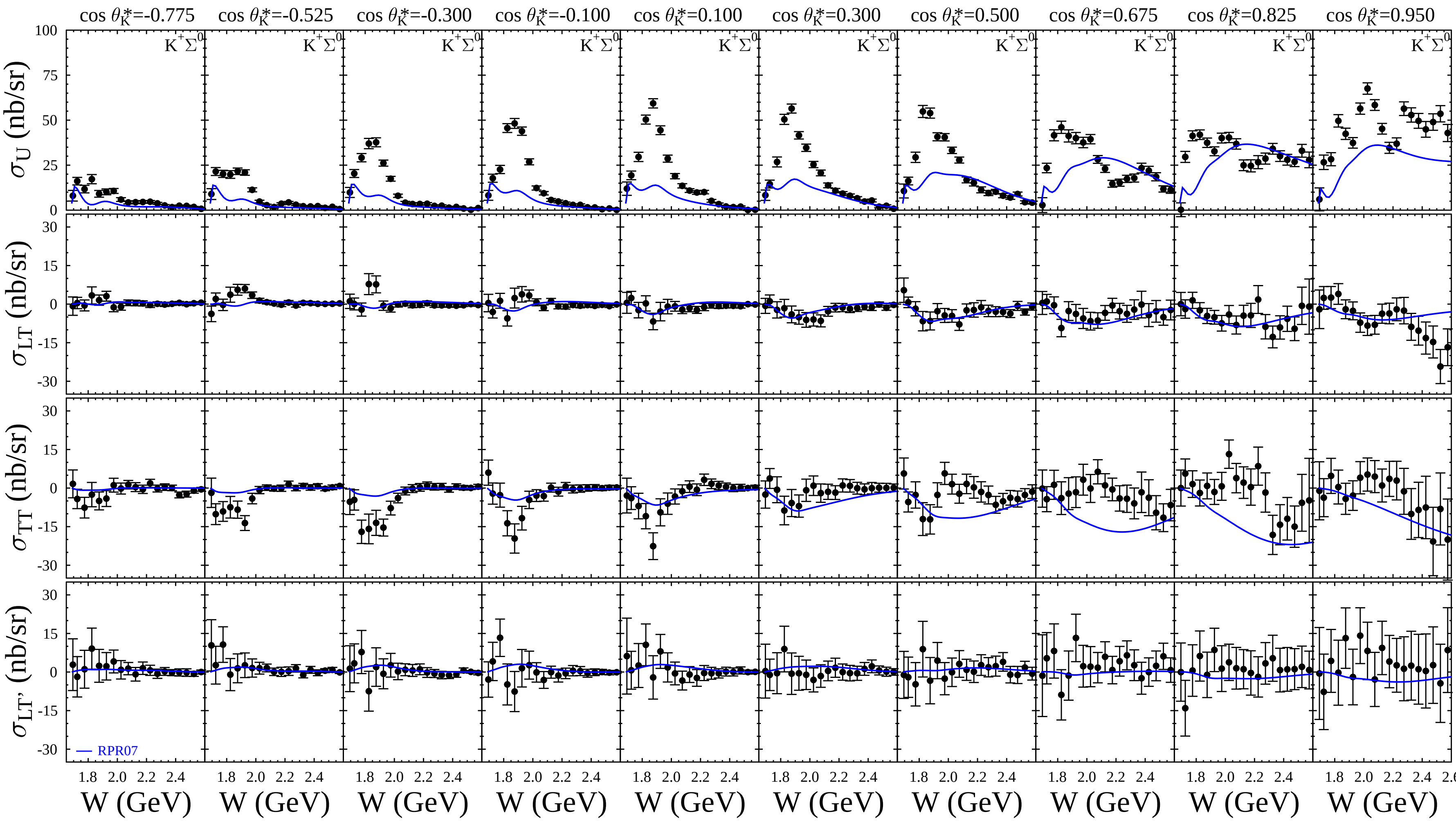

Figure 7: Structure functions $\sigma_U = \sigma_T + \epsilon\sigma_L$, σ_{LT}, σ_{TT}, and $\sigma_{LT'}$ (nb/sr) for $K^+\Sigma^0$ production vs. W (GeV) for E_b=5.5 GeV for Q^2=1.80 GeV^2 and $\cos\theta_K^*$ values as shown from CLAS data [39, 43]. The error bars represent the statistical uncertainties only. The blue curves are from the hybrid RPR-2007 KY model from Ghent [46].

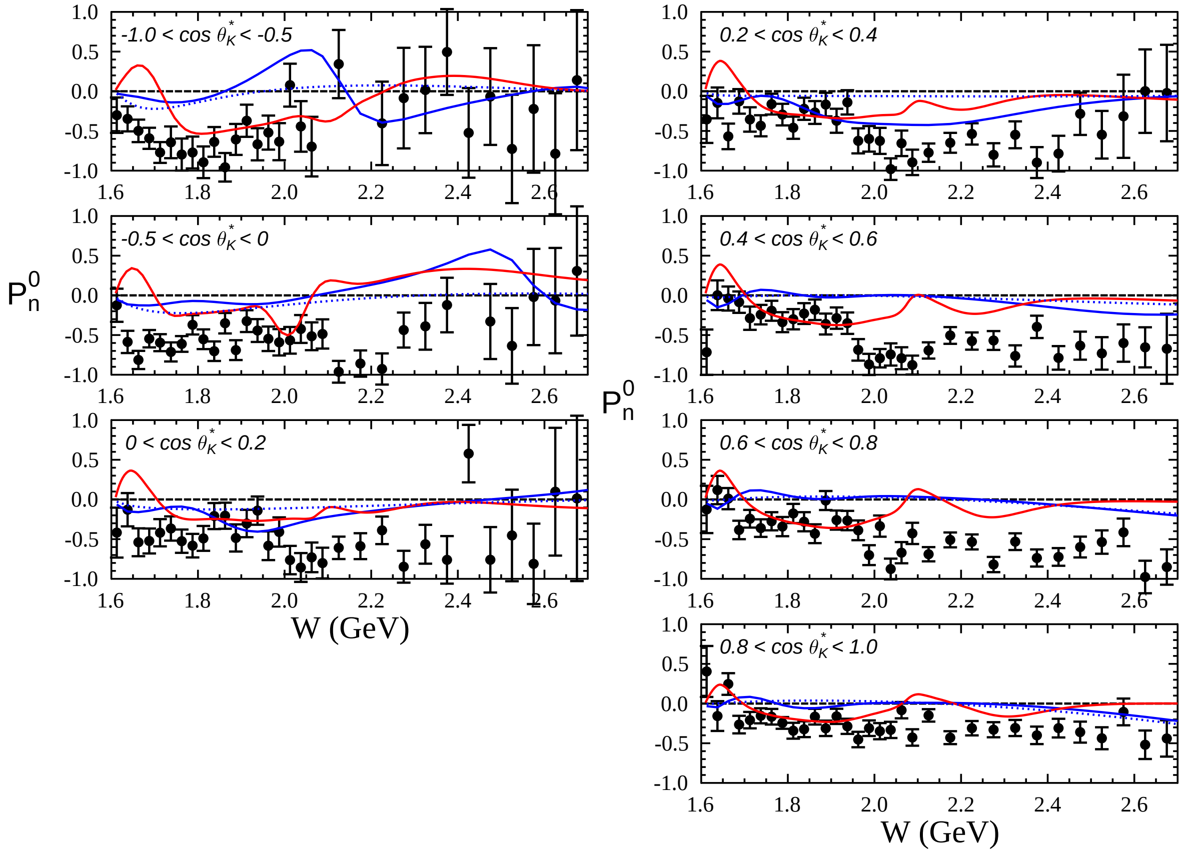

Figure 8: Induced polarization vs. W (GeV) for bins in $\cos\theta_K^*$ (as shown on the upper left of each plot) for an average $Q^2 = 1.9$ GeV^2 from CLAS $K^+\Lambda$ data [40]. The red curves are from the hadrodynamic KY model of Maxwell [44] and the blue curves are from the hybrid RPR-2011 KY model from Ghent [45].

KY provided for these states are less than 10% with uncertainties of the size of the measured coupling. While the relevance of this core set of N^* states in the $\gamma^{(*)}p \to K^+\Lambda$ reaction has long been considered a well-established fact, this set of states falls short of reproducing the experimental results for $W < 2$ GeV. A recent development in understanding the N^* spectrum was provided by the Bonn-Gatchina coupled-channel partial wave analysis of the final state reactions produced through the $N\pi$ and γp reactions [47]. This work presents an up-to-date listing of pole parameters and branching fractions for all N^* and Δ^* states up to $\sim$2 GeV with uncertainties at the level of a few percent. That analysis provided a list of six N^* states with coupling to $K\Lambda$, five N^* states with coupling to $K\Sigma$, and four Δ^* states with coupling to $K\Sigma$. For more on this list of states that couple to $K\Lambda$ and $K\Sigma$, see Ref. [48].

The findings of Ref. [47] are based on a significant amount of precision experimental data and a sophisticated coupled-channel fitting algorithm. However, in general, the issue of how to extract N^* content from open strangeness reactions is a long-standing question. Various analyses have led to very different conclusions concerning the set of resonances that contribute (e.g. compare results from Refs. [49, 50, 51], as well as the statements made regarding the resonant set from Ref. [47]). Furthermore, lack of sufficient experimental information, incomplete kinematic coverage, and underestimated systematics are still responsible for inconsistencies among the different models that fit the data to extract the contributing

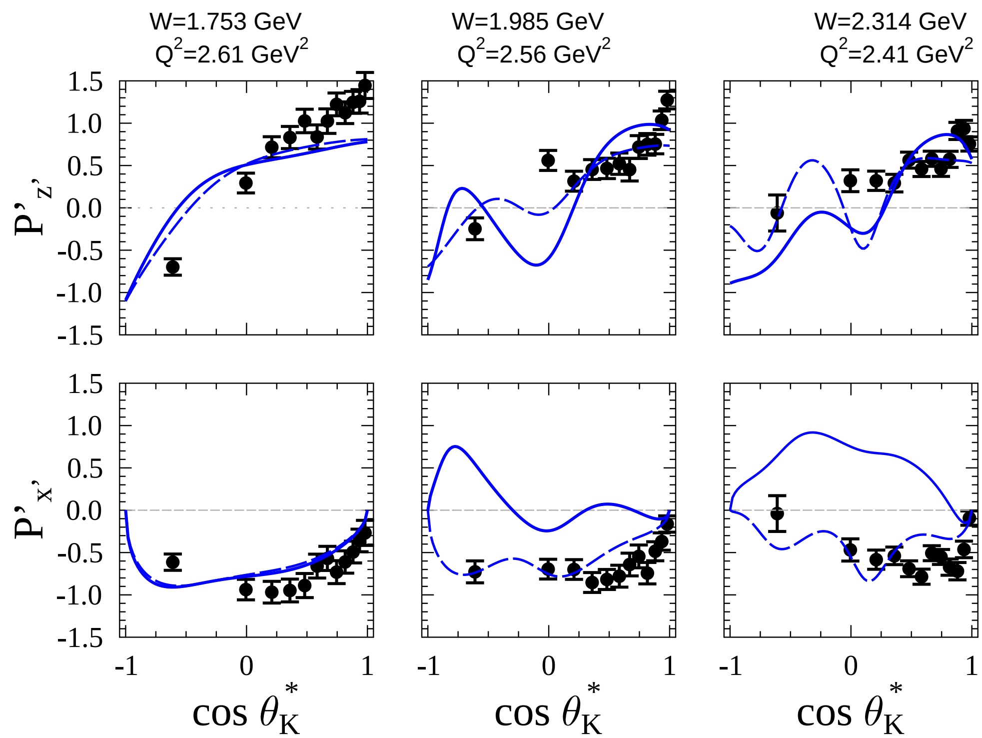

Figure 9: Beam-recoil transferred polarization data vs. $\cos\theta_K^*$ for representative bins in W and Q^2 from CLAS $K^+\Lambda$ data [42]. The curves are variants of the RPR-2007 model [46] including different N^* states at 1.9 GeV (dashed - D_{13}, solid - P_{11}).

resonances and their properties [51, 52]. The availability of precision electroproduction data to include in the fitting database to constrain the coupled-channel fits is expected to reduce the solution ambiguities and the algorithm dependence of the results.

3 CLAS12 N^* Program Objectives

The full experimental program of N^* studies with the CLAS12 detector has a number of important objectives. These include:

i) To map out the quark structure of the dominant N^* and Δ^* states from the data acquired for meson electroproduction through the exclusive final states including $p\pi^0$, $n\pi^+$, $p\eta$, $p\omega$, $p\pi^+\pi^-$, $K^+\Lambda$, and $K^+\Sigma^0$. This objective is motivated by results from existing analyses such as those shown in Fig. 4, where it is seen that the meson-baryon dressing contribution to the N^* structure decreases rapidly with increasing Q^2. The data can be described approximately in terms of dressed quarks already for $Q^2 \sim 5$ GeV^2. It is therefore expected that data that span from low to high Q^2 can map out the transition from the regime where low-energy degrees of freedom dominate to the regime where the quark core fully dominates the dynamics of the N^* and Δ^* states. The comparison of the extracted resonance electrocoupling parameters over this broad Q^2 regime to the predictions from LQCD and DSE calculations will allow for a much improved understanding of how the internal dressed quark core emerges from QCD and how the dynamics of the strong interaction are responsible for the formation of the N^* and Δ^* states of different quantum numbers.

ii) To investigate the dynamics of dressed quark interactions and how they emerge from QCD. This work is motivated by recent developments of hadronic models based on the DSE approach, and has provided links between the dressed quark propagator, the dressed quark scattering amplitudes, and the QCD Lagrangian. DSE analyses of the extracted N^* electrocoupling parameters have the potential to allow for investigation of the origin of dressed quark confinement in baryons and the nature of DCSB, since both of these phenomena are rigorously incorporated into DSE approaches [8, 11, 12].

iii) To study the Q^2-dependence of the non-perturbative dynamics of QCD. This is motivated by studies of the momentum dependence of the dressed quark mass function of the quark propagator within LQCD [53] and DSE [22, 23]. The calculated mass function approaches the current quark mass of a few MeV only in the high Q^2 regime of perturbative QCD. However, for decreasing momenta, the current quark acquires a constituent mass of $\sim$300 MeV as it is dressed by quarks and gluons. Verification of this momentum dependence would further advance understanding of non-perturbative dynamics. Efforts are currently underway to study the sensitivity of the proposed transition form factor measurements to different parameterizations of the momentum dependence of the quark mass [54].

iv) To offer constraints from resonance transition form factors for the $N \to N^*$ GPDs. We note that a key aspect of the CLAS12 measurement program is the characterization of exclusive reactions at high Q^2 in terms of GPDs. The elastic and $\gamma_v NN^*$ transition form factors represent the first moments of the GPDs [55, 56, 57], and they provide for unique constraints on the structure of nucleons and their excited states. Thus the N^* program at high Q^2 represents the initial step in a reliable parameterization of the transition $N \to N^*$ GPDs and is an important part of the larger overall CLAS12 program studying exclusive reactions. The studies of the CLAS results on $\gamma_v NN^*$ electrocouplings for the $N(1535)\frac{1}{2}^-$ resonance within the Light Cone Sum Rule approach coupled to LQCD have already provided access for the first time to parton degrees of freedom in the N^* structure in terms of quark distribution amplitudes [58].

The proposed experiment will complement these objectives. For the first time in a single experiment we will scan the Q^2 range below 5 GeV^2 where the contributions from both the meson-baryon cloud and quark core are relevant and the Q^2 range above 5 GeV^2 where the quark core dominance is expected with the final states that require the creation of an $s\bar{s}$ pair. It offers a unique opportunity to explore the emergence of the external meson-baryon cloud from the core of confined quarks and gluons and to check the theoretical expectations on the meson-baryon cloud generation from the confinement regime.

4 Experiment Details

4.1 Experimental Overview

The CLAS12 spectrometer [59] is designed for operation at beam energies up to 11 GeV (the maximum possible for delivery to Hall B) and will operate at a nominal beam-target luminosity of 1×10^{35} cm^{-2}s^{-1}, an order of magnitude increase over previous CLAS operation. This luminosity will allow for precision measurements of cross sections and polarization observables for many exclusive reaction channels for invariant energies W up to 3 GeV, the full decay product phase space, and four-momentum transfers Q^2 up to 12 GeV^2. The physics program for CLAS12 focuses on measurements of the spatial and angular momentum structure of the nucleon, investigation of quark confinement and hadron mass generation in the spectrum and structure of the ground- and excited-state nucleons, and studies of the strong interaction in nuclei. The CLAS12 physics program currently consists of 9 separate run groups. However, at the present time, there is no approved beam time at lower incident electron beam energies.

We plan to measure the exclusive $K^+\Lambda$ and $K^+\Sigma^0$ final states from a liquid-hydrogen target with the CLAS12 spectrometer using a longitudinally polarized electron beam. The experiment will operate with the torus at the maximum possible current (assumed to be $B = 0.9B_{max}$ or I=3375 A) set with a polarity such that negatively charged particles bend away from the electron beamline. These parameters are fully consistent with those for the other experiments that are part of this new proposed run group. At incident beam energies of 6.6 GeV and 8.8 GeV, we will measure the differential cross sections and hyperon polarization components over a range of invariant energies 1.6 GeV $< W <$ 3 GeV in the domain of momentum transfers Q^2 from 2 GeV^2 to 7 GeV^2, while spanning the full center-of-mass angular range of the final state K^+. Measurements in the range of $Q^2 < 4$ GeV^2 will provide significant overlap to connect to the existing CLAS KY data from Refs. [36, 37, 38, 39, 40, 41, 42]. In fact, these data for $Q^2 < 4$ GeV^2 will actually well extend the observables already published from analysis of the CLAS electroproduction data highlighted in Section 2.2 in Figs. 6 to 9 due to the significant factor of increase in the expected statistics compared to the CLAS data of $\sim$10 at Q^2=4 GeV^2 and $\sim$100 at Q^2=2 GeV^2. The data in the range from Q^2=4 GeV^2 to 7 GeV^2 provides the bridge of new data to overlap with the high Q^2 data from E12-106-108A that will take data at a beam energy of 11 GeV during the first CLAS12 physics running period scheduled to take data in 2017.

4.2 Stage 1 Analysis

The first stage of the analysis of the experimental data will be to extract the differential cross sections, the separated structure functions, and the induced and transferred polarizations for the $K^+\Lambda$ and $K^+\Sigma^0$ final states. In this section the specific observables to be measured and the path to their extraction from the measured data are detailed.

Following the notation of Refs. [39, 42, 60], for the case of an unpolarized electron beam (helicity h=0) with no target or recoil polarizations, the virtual photon cross section for the K^+Y electroproduction reaction can be written (using simplifying notation for the differential cross section) as:

$$\frac{d\sigma}{d\Omega_K^*} \equiv \sigma_0 = \sigma_U + \epsilon\sigma_{TT}\cos 2\Phi + \sqrt{\epsilon(1+\epsilon)}\sigma_{LT}\cos\Phi, \tag{1}$$

where σ_i are the structure functions that measure the response of the hadronic system and $i = T$, L, LT, and TT represents the transverse, longitudinal, and interference structure functions. The structure functions are, in general, functions of Q^2, W, and θ_K^* only. In this work the unseparated structure function is defined as $\sigma_U = \sigma_T + \epsilon\sigma_L$. Here Φ is the angle between the electron scattering plane and the KY hadronic reaction plane and ϵ is the virtual photon parameter defined as:

$$\epsilon = \left(1 + 2\frac{\nu^2}{Q^2}\tan^2\frac{\theta_{e'}}{2}\right)^{-1}. \tag{2}$$

Here $\theta_{e'}$ is the electron scattering angle in the laboratory frame and ν is the energy transfer of the virtual photon. Fig. 10 shows the kinematics for the KY electroproduction reaction in the γ^*-target proton center-of-mass (CM) frame and the coordinate system employed for the polarization formalism.

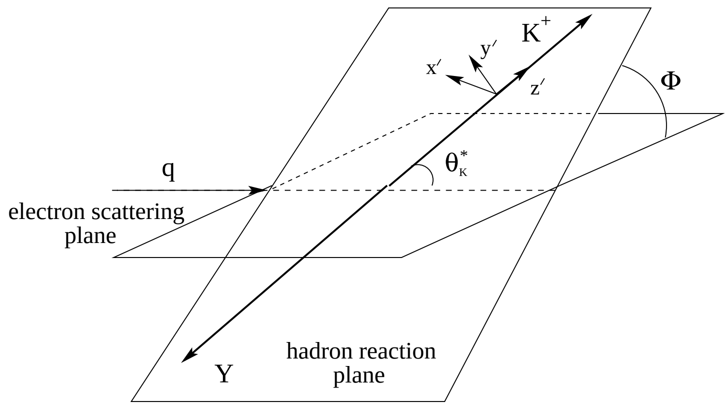

Figure 10: Kinematics for KY electroproduction defining the angles θ^*_K and Φ, as well as the coordinate system used to define the polarization formalism. This figure shows a positive Φ angle.

For the case of a polarized electron beam with helicity h, the cross section form of Eq.(1) is modified to include an additional term:

$$\frac{d\sigma}{d\Omega^*_K} = \sigma_0 + h\sqrt{\epsilon(1-\epsilon)}\sigma_{LT'}\sin\Phi. \tag{3}$$

The electron beam polarization produces a fifth structure function $\sigma_{LT'}$ that is related to the beam helicity asymmetry via:

$$A_{LT'} = \frac{\frac{d\sigma^+}{d\Omega^*_K} - \frac{d\sigma^-}{d\Omega^*_K}}{\frac{d\sigma^+}{d\Omega^*_K} + \frac{d\sigma^-}{d\Omega^*_K}} = \frac{\sqrt{\epsilon(1-\epsilon)}\sigma_{LT'}\sin\Phi}{\sigma_0}, \tag{4}$$

where the $\pm$ superscripts on $\frac{d\sigma}{d\Omega^*_K}$ correspond to the electron helicity states of $h = \pm 1$.

The polarized structure function $\sigma_{LT'}$ is intrinsically different from the structure functions of the unpolarized cross section. This term is generated by the imaginary part of terms involving the interference between longitudinal and transverse components of the hadronic and leptonic currents, in contrast to σ_{LT}, which is generated by the real part of the same interference. $\sigma_{LT'}$ is non-vanishing only if the hadronic tensor is antisymmetric, which will occur in the presence of rescattering effects, interferences between multiple resonances, interferences between resonant and non-resonant processes, or even between non-resonant processes alone [61]. $\sigma_{LT'}$ could be non-zero even when σ_{LT} is zero. When the reaction proceeds through a channel in which a single amplitude dominates, the longitudinal-transverse response will be real and $\sigma_{LT'}$ will vanish. Both σ_{LT} and $\sigma_{LT'}$ are necessary to fully unravel the longitudinal-transverse response of the K^+Y electroproduction reactions.

The bin-centered differential cross section for each hyperon final state in each kinematic bin i is computed using the form:

$$\frac{d\sigma_i}{d\Omega_K^*} = \frac{1}{\Gamma_v} \cdot \frac{1}{(\Delta Q^2 \Delta W \Delta \cos\theta_K^* \Delta\Phi)} \cdot \frac{R_i \cdot N_i \cdot BC_i}{\eta_i \cdot N_0} \cdot \frac{1}{(N_A \rho t / A_w)}, \tag{5}$$

where Γ_v is the virtual photon flux factor given by:

$$\Gamma_v = \frac{\alpha}{4\pi} \frac{W}{M_p^2 E^2} \frac{W^2 - M_p^2}{Q^2} \frac{1}{1-\epsilon} \tag{6}$$

is the flux of virtual photons (using the definition from Ref. [62]) for each bin at the bin-averaged mean of the bin and $\Delta Q^2 \Delta W \Delta \cos\theta_K^* \Delta\Phi$ is the volume of the analysis bin (with bin sizes corrected for kinematic limits in the threshold W bins), R_i is the radiative correction factor, N_i is the background-subtracted K^+Y yield in each bin, BC_i is the factor that evolves the measured bin-averaged differential cross section over each bin to a specific kinematic point within the Q^2, W, $\cos\theta_K^*$, Φ bin, and η_i accounts for the detector geometrical acceptance and efficiency corrections. N_0 is the live-time corrected incident electron flux summed over all data runs included in this analysis determined from the Faraday Cup charge. Finally, $N_A \rho t / A_w$ represents the target number density, where N_A is Avogadro's number, ρ is the target density, t is the target length, and A_w is the atomic weight of the target.

As for all electroproduction data, the raw cross sections will be subjected to radiative corrections in order to extract the final differential cross sections. The radiative correction procedure for exclusive processes is well established [63], and has been used in all of the analyses of the CLAS electroproduction cross sections. As it has been recently demonstrated [34], radiative corrections are very important for the analysis of exclusive processes in terms of resonance excitations as they affect both the polar and azimuthal angular dependencies. This is particularly important in the extraction of the separated U, LT, and TT structure functions from the differential cross sections, which involves a Φ moment analysis (see e.g. Refs. [34, 37, 39]).

Fits to the Φ dependence of the differential cross sections for the $K^+\Lambda$ and $K^+\Sigma^0$ final states will be carried out to determine the separated structure functions $\sigma_U \equiv \sigma_T + \epsilon\sigma_L$, σ_{TT}, and σ_{LT}. Fits to the beam spin asymmetry will be carried out to determine the polarized structure function $\sigma_{LT'}$. The separated structure functions will be extracted as a function of Q^2, W, and $\cos\theta_K^*$, using the well-established techniques that were developed from analyses of these same final states from the CLAS program [37, 39]. Note that a separation of σ_L and σ_T is not required for this proposal as the longitudinal amplitudes can be probed with greater sensitivity from the interference structure functions σ_{LT} and $\sigma_{LT'}$. In actuality a Rosenbluth separation is not practical in these kinematics at E_b=6.6 GeV and 8.8 GeV due to the limited ϵ lever arm.

In the $K^+\Lambda$ reaction, the Λ decays weakly into a pion and a nucleon. Due to the nature of the weak decay, the decay nucleons are constrained to move preferentially in the direction of the hyperon spin. More precisely, the mesonic decay of the free Λ has an asymmetric angular distribution with respect to the spin direction of the Λ. This asymmetry is the result of an interference between parity non-conserving (s-wave) and parity-conserving (p-wave) amplitudes. In the hyperon CM frame, the decay nucleon angular distribution is therefore of the form [64]:

$$\frac{dN}{d\cos\theta_p^{RF}} = N(1 + \alpha_\Lambda P_\Lambda \cos\theta_p^{RF}), \tag{7}$$

where P_Λ is the magnitude of the Λ polarization and θ_p^{RF} is the angle between the polarization axis and the decay proton momentum in the Λ rest frame. The parameter α_Λ is the weak decay asymmetry parameter given by α_Λ=0.642 [14]. This analysis will exclusively study the dominant $p\pi^-$ decay branch (B.R.=64%) of the Λ hyperon. For the $K^+\Sigma^0$ reaction, the Σ^0 follows the decay chain $\Sigma^0 \to \gamma\Lambda$ (B.R.=100%), with $\Lambda \to N\pi$. Again, the angular distribution of the decay nucleon from the Λ follows from Eq.(7). However, α_Λ is replaced by $\alpha_\Sigma = -0.164$ (see Ref. [42] for details).

The hyperon polarization is a vector whose components can be projected onto a set of coordinate axes, referred to as the spin-quantization axes. For the formalism provided here, the primed-coordinate system of Fig. 10 has been chosen. Each of the hyperon polarization components, $P_{x'}$, $P_{y'}$, and $P_{z'}$, can be split into a beam helicity-independent part, called the *induced* polarization, and a beam helicity-dependent part, called the *transferred* polarization. This can be written as:

$$P_{i'} = P_{i'}^0 + hP_{i'}'. \tag{8}$$

To accommodate finite bin sizes and to improve statistics, our analysis will be performed by summing over all relative angles Φ between the electron and hadron planes just as was done for the analyses of Refs. [41, 42]. Using the script symbol $\mathcal{P}$ to represent the Φ-integrated Λ polarization components, they can be expressed in the (x', y', z') system in terms of the response functions as shown in Table 1 [42]. In performing the integration over Φ, the polarization components $\mathcal{P}_{x'}^0$, $\mathcal{P}_{z'}^0$, and $\mathcal{P}_{y'}'$ are equal to zero. In Table 1, the normalization term $K_I = 1/(R_T^{00} + \epsilon R_L^{00})$.

$\mathcal{P}_{x'}^0$	0	$\mathcal{P}_{x'}'$	$K_I\sqrt{1-\epsilon^2}R_{TT'}^{x'0}$
$\mathcal{P}_{y'}^0$	$K_I(R_T^{y'0} + \epsilon R_L^{y'0})$	$\mathcal{P}_{y'}'$	0
$\mathcal{P}_{z'}^0$	0	$\mathcal{P}_{z'}'$	$K_I\sqrt{1-\epsilon^2}R_{TT'}^{z'0}$

Table 1: Hyperon polarization components $\mathcal{P}_i$ in the (x', y', z') system integrated over Φ.

The induced polarization in a given Q^2, W, $\cos\theta_K^*$ kinematic bin for a given coordinate can be extracted by forming the forward-backward yield asymmetry with respect to $\cos\theta_p^{RF} = 0$. Integrating Eq.(7) from 0 to 1 (forward) and -1 to 0 (backward) gives the corresponding yields N^F and N^B. The induced polarization can be expressed in terms of the forward-backward asymmetry A_i with respect to a given spin-quantization axis $i = x', y', z'$ using

$$\mathcal{P}_i^0 = \frac{2A_i}{\alpha} = \frac{2}{\alpha}\frac{N^F - N^B}{N^F + N^B}. \tag{9}$$

For the beam-recoil transferred polarization measurement, Eq.(7) is used forming the beam helicity-gated asymmetry for a given kinematic bin with respect to a given spin quantization axis i as:

$$A_i = \frac{N^+ - N^-}{N^+ + N^-} = \alpha P_b \mathcal{P}' \cos\theta_p^{RF}, \tag{10}$$

The slope of a linear fit to the A_j vs. $\cos\theta_p^{RF}$ distribution then yields the transferred hyperon polarization components

4.3 Stage 2 Analysis

In the second stage of the analysis, the N^* and Δ^* electrocoupling parameters will be extracted from fits to the separated structure function and polarization data using either an existing reaction model such as the Regge plus resonance model from Ghent [46] (updated to provide for a reasonable description of the data) or a phenomenological approach that is analogous to those developed in recent years for analysis of the CLAS $N\pi$ and $N\pi\pi$ datasets. These include the UIM isobar model [65] and an approach based on dispersion relations for the $N\pi$ channel [66]. For the $N\pi\pi$ channel the JM isobar model has been developed [67, 68]. The extraction of the electrocoupling amplitudes will be completed separately for both the $K^+\Lambda$ and $K^+\Sigma^0$ channels as a function of Q^2. These results can be compared with the $\gamma_v NN^*$ electrocouplings available from the studies of the $N\pi\pi$ channel. These fits will provide a set of initial N^* electrocoupling amplitudes. A final evaluation of N^* electrocoupling amplitudes will be carried out within the framework of the most advanced coupled-channel approaches, which are currently being developed by the Argonne-Osaka Collaboration [7] and the GWU group [69] (members of which are part of the group supporting this proposal). Both of these approaches account for the contributions of all relevant meson-baryon open channels and their hadronic interactions. Ultimately, they will include updates from JPARC data on the (π, K) and (K, π) reaction channels at W values covered by this proposal [70]. Consistent results on the $\gamma_v NN^*$ electrocouplings from independent analyses of the $N\pi$, $N\pi\pi$ and KY channels and extracted from the global coupled-channel analysis will provide the final reliable extraction of these fundamental quantities.

4.4 Monte Carlo Simulation Studies

In order to study the detector response and to model the CLAS12 acceptance function for this proposal, the standard CLAS12 fast Monte Carlo (fastMC) suite was employed. This simulation code included the nominal detector geometries and the expected position and time resolutions for the detectors for the reconstruction of the four-momenta of the final state particles. The event generator was based on the PYTHIA6 phase space model modified to reflect the expected Q^2 dependence of the incident virtual photon flux and the t-dependence ($t = (p_{\gamma^*} - p_K)^2$) of the final state K^+ seen from Ref. [39]. Fig. 11 shows the kinematics of the reconstructed Monte Carlo events at a beam energy E_b=6.6 GeV as a function of Q^2, W, and $\cos\theta_K^*$. The corresponding distributions of these quantities reconstructed from the CLAS e1f dataset at E_b=5.5 GeV are shown in Fig. 12 for comparison. Fig. 11 shows that the Q^2 and W distributions match qualitatively to the CLAS e1f data from Fig. 12.

The differences are due to different beam energies (6.6 GeV vs. 5.5 GeV) and due to the use of the phase-space event generator. The $\cos\theta_K^*$ distribution from Monte Carlo shows the strong forward-peaking as the CLAS data but has two notable features. The first is a different behavior as $\cos\theta_K^* \to 1$ due to the different torus polarities (the CLAS12 simulations used a negative torus polarity and the CLAS data was taken with a positive torus polarity). The second is a dip at $\cos\theta_K^* \approx -0.2$ due to the acceptance gap between the CLAS12 forward and central detectors that is exacerbated by the negative torus polarity. The p vs. θ laboratory distributions for the final state charged particles e', K^+, p, and π^- are shown in Fig. 13. The e', K^+, and p are mostly directed toward the CLAS12 forward detector system ($\theta < 35°$), while the π^- tracks are mostly contained within the CLAS12 central detector system ($\theta > 35°$).

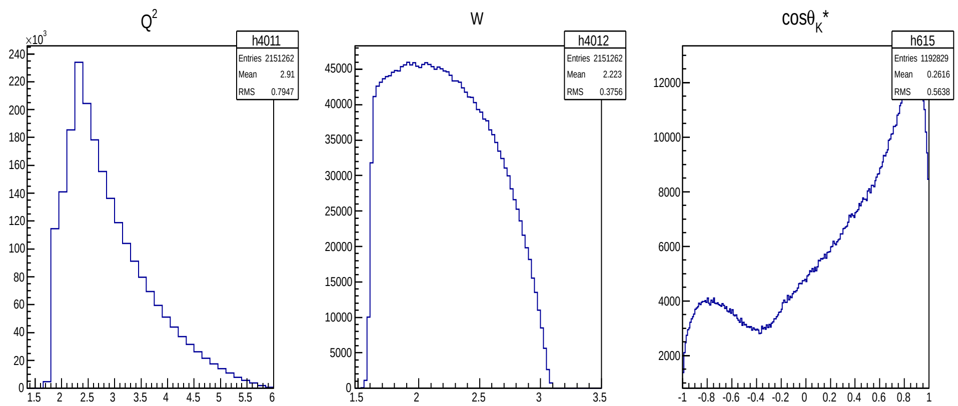

Figure 11: Yield distributions of Q^2, W, and $\cos\theta_K^*$ for the reconstructed Monte Carlo events from the modified K^+Y phase space generator at E_b=6.6 GeV with the torus set at $B = 0.9B_{max}$ for negatively charged particles outbending used to determine the CLAS12 acceptance functions for this proposal. Note that the sharp edges seen in the Q^2 and W distributions here are due to the kinematic bounds selected for the event generation.

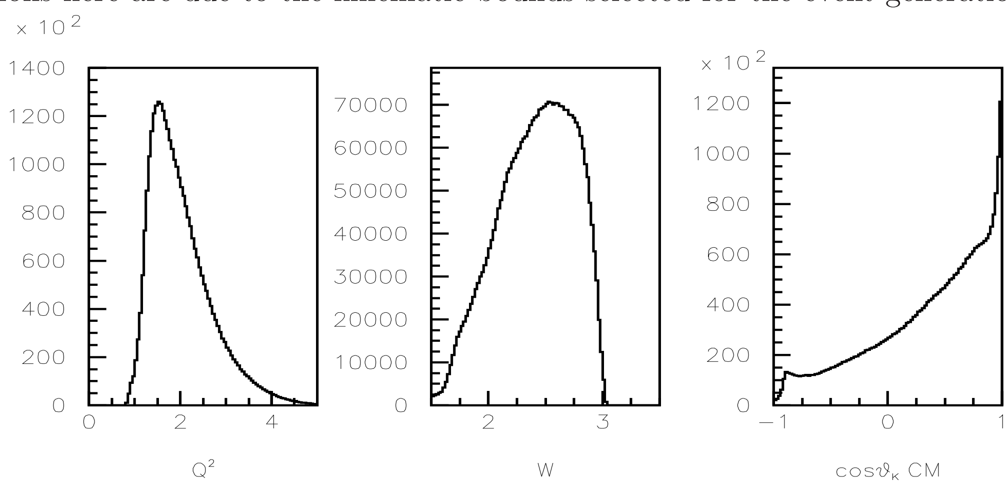

Figure 12: Yield distributions of Q^2, W, and $\cos\theta_K^*$ for the CLAS e1f dataset at E_b=5.5 GeV for K^+Y events with the torus set at $B = 0.9B_{max}$ with negatively charged particles inbending.

The momentum distribution for the final state K^+ is important to consider given the particle identification capabilities of CLAS12. The reconstructed K^+ momenta will be in

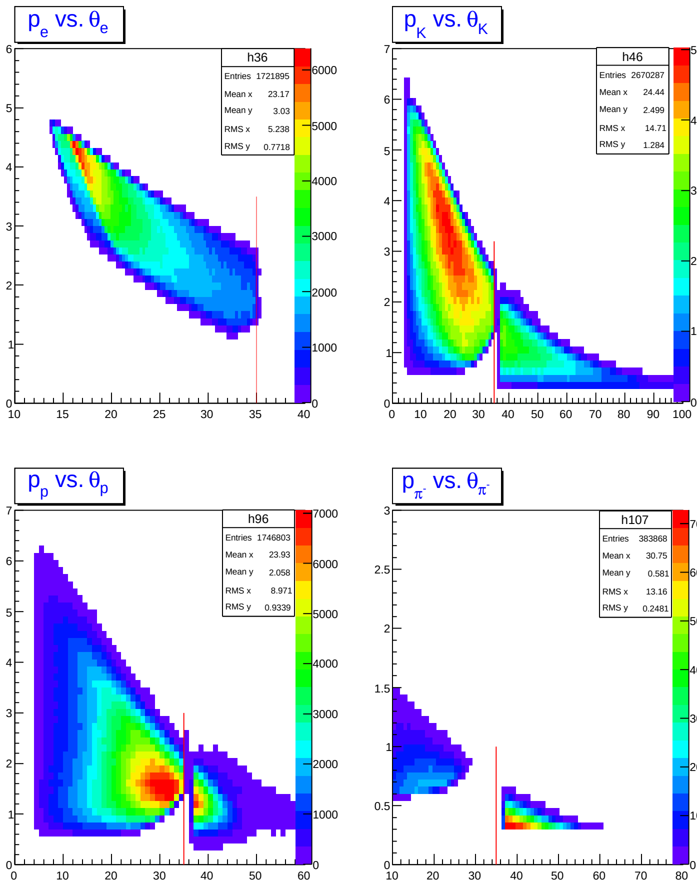

Figure 13: Yield distributions of laboratory momentum (GeV) vs. polar angle (deg) for the final state e' (UL), K^+ (UR), p (LL), and π^- (LR) for the reaction $ep \to e'K^+\Lambda$ at E_b=6.6 GeV with the torus set at $B = 0.9B_{max}$ for negatively charged particles outbending. The discontinuity at $\theta = 35°$ (noted by the vertical red lines) is due to the acceptance gap between the CLAS12 forward and central detectors.

the range from 0.5 GeV to 7 GeV. Fig. 14 shows the K^+ momenta as a function of Q^2 from our Monte Carlo data over the kinematic range of this proposal. The average K^+ momentum is $\sim 2-4$ GeV, with a relatively weak dependence on Q^2.

Figure 15 shows the particle identification capabilities expected for the CLAS12 Forward Time-of-Flight (FTOF) system based on the flight time differences between charged hadrons as a function of momentum. The primary issue with the final state reconstruction will be separating K^+ tracks from the dominant π^+ background. The FTOF system was designed to separate K^+ tracks from π^+ tracks up to ∼3 GeV with 4σ separation (assuming an average FTOF resolution of 80 ps). However, 1σ separation based on the nominal system design up to 6 GeV is provided. However, these statements are believed to be *extremely* conservative. Based on the measured resolutions for the new FTOF panel-1b counters, 2σ separation of π/K tracks up to 6 GeV should be achievable. The average timing resolution of the new FTOF panel-1b system is ∼50 ps (δt=30 ps at small angles to 80 ps at large angles). The timing resolution of the FTOF system is expected to improve by an additional ∼20% when the timing information from the panel-1b arrays is combined with that for the panel-1a arrays located immediately downstream of panel-1b. Details on the FTOF system

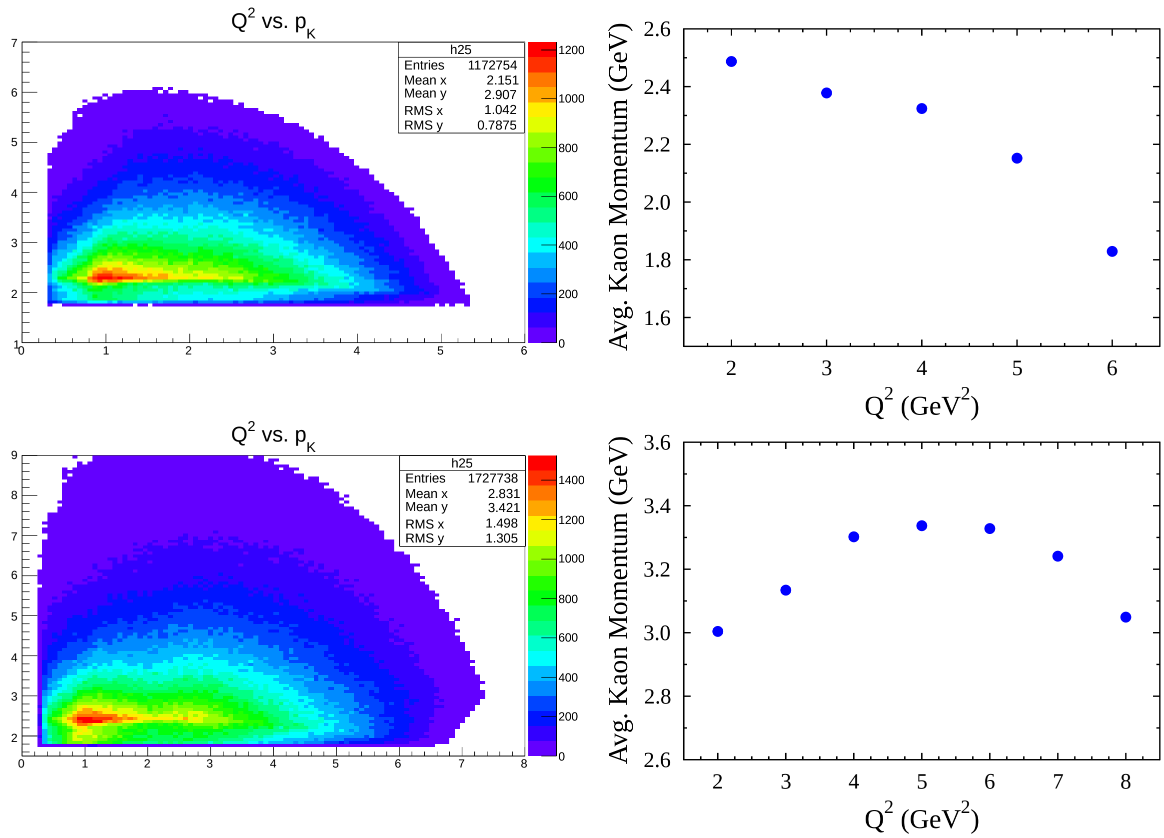

Figure 14: Yield distributions of Q^2 vs. K^+ momentum (left) and the average K^+ momentum vs. Q^2 (right) for E_b=6.6 GeV (top) and E_b=8.8 GeV (bottom) with the torus set at $B = 0.9B_{max}$ for negatively charged particles outbending for K^+Y events.

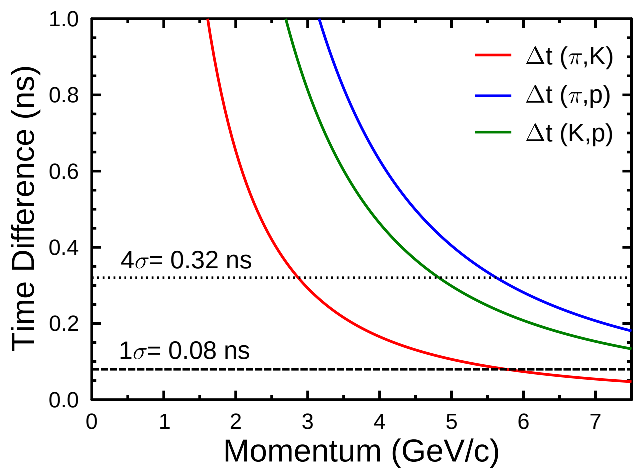

Figure 15: Difference in charged hadron flight times from the event vertex to the FTOF system as a function of hadron momentum showing the differences between π/K (red curve), π/p (blue curve), and K/p (green curve). The 4σ and 1σ FTOF time resolution lines are shown.

performance are available in Ref. [71]. Final state K^+ identification will thus rely heavily on the FTOF particle identification capabilities over the full K^+ momentum range.

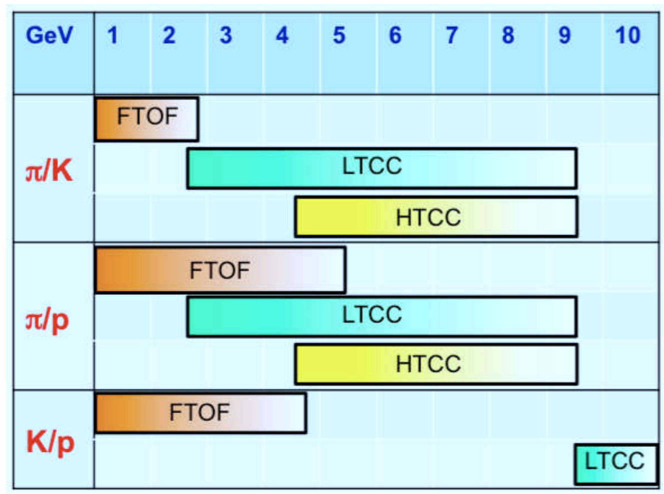

Figure 16: Representation of which CLAS12 subsystems are employed for charged hadron identification as a function of momentum.

Particle identification in CLAS12 in the forward direction is actually accomplished through the use of multiple detection subsystems, including not only the FTOF, but also the two Cherenkov detector systems, the Low Threshold Cherenkov Counter (LTCC) and the High Threshold Cherenkov Counter (HTCC). Fig. 16 shows a representation of which subsystems are nominally employed for charged hadron identification as a function of momentum. The LTCC in its nominal active area is expected to be 95% - 99% efficient for π/K separation in the range of momenta from 3 GeV to 9 GeV. The HTCC is expected to be 95% - 99% efficiency for π tracks from 5 GeV to 9 GeV.

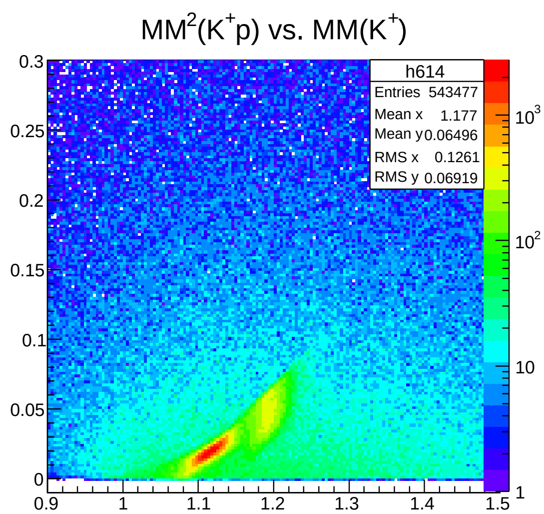

Figure 17: Correlation of the reconstructed $MM^2(e'K^+p)$ (GeV^2) vs. $MM(e'K^+)$ (GeV) distributions at E_b=6.6 GeV with the torus set at $B = 0.9B_{max}$ for negatively charged particles outbending.

The nominal analysis scheme will identify the exclusive reaction channel by detection of the final state e' and K^+. However, the detection of the final state proton from the Λ hyperon mesonic decay (B.R.=63.9%) will allow us to further reduce the underlying backgrounds employing a cut on the $MM^2(e'K^+p)$ distribution to select events with a missing π^- or a missing $\pi^-\gamma$ (see Fig. 17). This will allow for fits that separate the $K^+\Lambda$, $K^+\Sigma^0$, and background contributions with different systematics. Comparison of cross sections extracted using the $e'K^+$ final state topology to that from the $e'K^+p$ final state topology will be used to assess the systematic uncertainties associated with the background subtraction and fitting algorithms used to separate the $K^+\Lambda$ and $K^+\Sigma^0$ event samples from the $e'K^+$ missing mass distributions for each bin of Q^2, W, $\cos\theta_K^*$, and Φ.

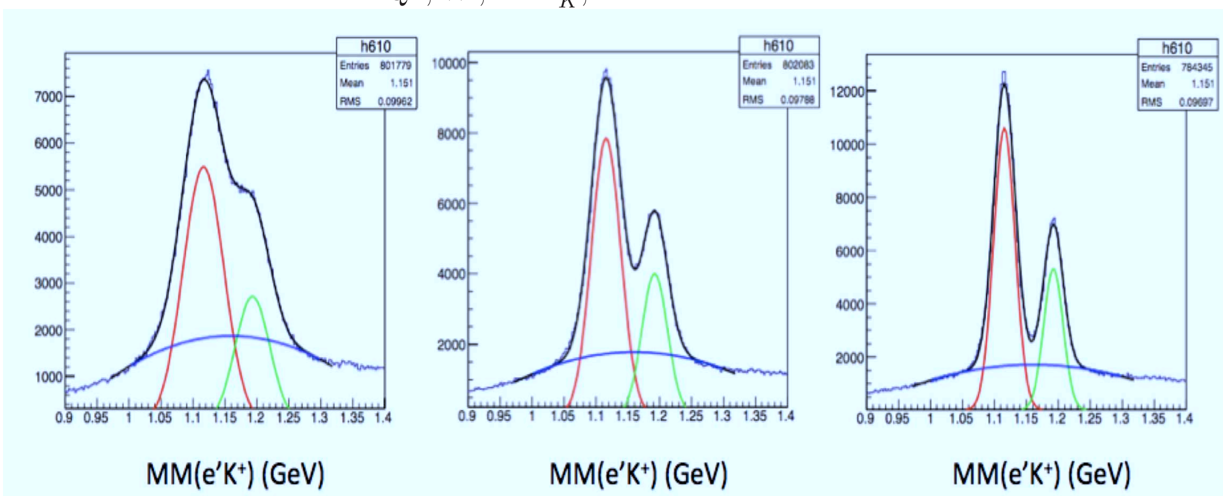

Figure 18: Missing mass spectra $MM(e'K^+)$ for the reconstructed $e'K^+p$ final state topology for reversed torus magnet polarity with $B = 0.4B_{max}$ (left), $B = 0.60B_{max}$ (middle), and $B = 0.9B_{max}$ (right) for the expected ratios of $K^+\Lambda$, $K^+\Sigma^0$, and background events. The histograms are overlaid with lineshape fits.

For this proposal the fastMC studies have shown that the CLAS12 acceptance for both $e'K^+$ and $e'K^+p$ final states is fairly flat for torus field settings from $B = 0.4B_{max}$ to $B = 0.9B_{max}$. The acceptance for positive polarity torus operation (negatively charged particles bending inward) is seen to be ~10% higher than for reversed field running. However, the reversed torus polarity configuration has been assumed in the Monte Carlo studies as this is the configuration that has been chosen for this run group. However, while the acceptance dependence on the torus configuration is relatively small, the biggest affect on the KY analysis versus torus field strength is the missing mass resolution function. The average CLAS12 missing mass resolution at $0.4B_{max}$ is 30 MeV, at $0.6B_{max}$ is 22 MeV, and at $0.9B_{max}$ is 15 MeV. Representative hyperon missing mass spectra for the detected $e'K^+p$ final state topology are shown in Fig. 18. For these studies, three different reactions were simulated, including the hyperon channels of interest, $K^+\Lambda$ and $K^+\Sigma^0$, as well as the predominant background channel $ep \to e'p\pi^+\pi^-$, where the final state π^+ is misidentified as a K^+. These studies employed $N_{K\Lambda}/N_{K\Sigma}$=2 based on the ratios seen in the CLAS e1c and e1f datasets (which span 0.5 GeV^2 < Q^2 < 3.9 GeV^2, W up to 2.6 GeV). The background channel was assumed to have three times the integrated yield as the $K^+\Lambda$ channel in the mass range shown, again based on the findings from the CLAS e1c and e1f datasets scaled by the expected particle misidentification background expected for CLAS12 operation at $\mathcal{L} = 1 \times 10^{35}$ cm^{-2}s^{-1} (see Section 4.5).

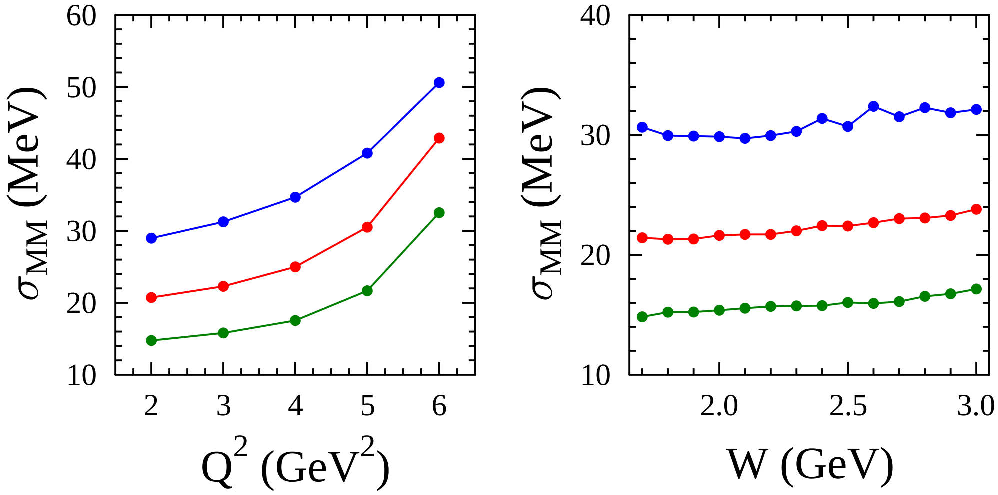

Figure 19: Hyperon missing mass $MM(e'K^+)$ resolution from reconstructed $ep \to e'K^+\Lambda$ Monte Carlo data as a function of (left) Q^2 (averaged over W and $\cos\theta_K^*$) and (right) W (averaged over Q^2 and $\cos\theta_K^*$). The blue curves are for $B = 0.4B_{max}$, the red curves are for $B = 0.60B_{max}$, and the green curves are for $B = 0.9B_{max}$.

Figure 19 shows the expected missing mass resolution of CLAS12 as a function of Q^2 and W summed over all other kinematic variables at E_b=6.6 GeV for the 3 torus field strengths of 40%, 60%, and 90% B_{max}. The resolution is relatively flat with W. However, the resolution function has a strong dependence on Q^2. Further work will be needed to develop approaches for fitting the missing mass spectra to separate the $K^+\Lambda$, $K^+\Sigma^0$, and background channels. However, the algorithms successfully employed for the analysis of Ref. [39] will be used as a starting point. Note as well that the fastMC does not account for radiative effects that will increase the degree of overlap of the hyperon peaks in the $MM(e'K^+)$ spectrum. However, in these kinematics the radiative effects are not expected to significantly affect the spectrum as reflected in Fig. 18.

Separation of the $K^+\Lambda$ and $K^+\Sigma^0$ event samples will proceed using a fitting approach that accounts for the CLAS12 resolution function as a function of Q^2 and W as alluded to above. With detection of only the final state $e'K^+$ or $e'K^+p$, kinematic fitting does not have sufficient constraints to enable a complete event-by-event separation of the $K^+\Lambda$, $K^+\Sigma^0$, and background channels. In fact, kinematic fitting is not expected to lead to any significant improvement relative to a careful spectrum fitting approach. However, investigations of kinematic fitting approaches and studies of their effectiveness for CLAS12 and for these specific final states are now being considered.

4.5 Event Backgrounds

The backgrounds within the $e'K^+$ missing mass distributions need careful consideration in the planning of this experiment. If the CLAS12 K^+ particle identification in the event reconstruction was certain (i.e. C.L.=100%), then the contributing backgrounds could easily be eliminated. However, there will always be a finite probability of making the wrong particle assignment in the final state reconstruction. Using a particle identification scheme based solely on timing information from the FTOF detectors, there are two possible avenues to misidentify a K^+ and a π^+:

1. The finite time resolution of the FTOF system cannot distinguish π^+ and K^+ tracks when their flight time difference for a given momentum is on the order of the system timing resolution (see Fig. 15).

2. π^+ tracks from earlier or later beam buckets when associated with the beam bucket of the triggering electron can appear to be K^+ tracks.

For particle misidentification of the first sort, the better the system timing resolution, the smaller this contribution will be. However, for events of the second sort, the misidentification probability is not dependent on the system timing resolution.

The K^+ misidentification background will reside in the $e'K^+$ missing mass distribution and a predominant component will arise from accidental coincidences between scattered electrons and unrelated hadrons. These unrelated hadrons are primarily pions from neighboring beam bunches. Of course the other important contribution will be from physics backgrounds, the dominant reaction process being $ep \to e'\pi^+\pi^-p$, where the π^+ is misidentified as a K^+. Fig. 20 shows the reconstructed $MM(e'K^+)$ distributions from CLAS data at E_b=5.5 GeV for the two final state topologies of interest, $e'K^+$ and e', K^+, p. Note that the backgrounds beneath the hyperon peaks are significantly reduced with the inclusion of the detection of the proton.

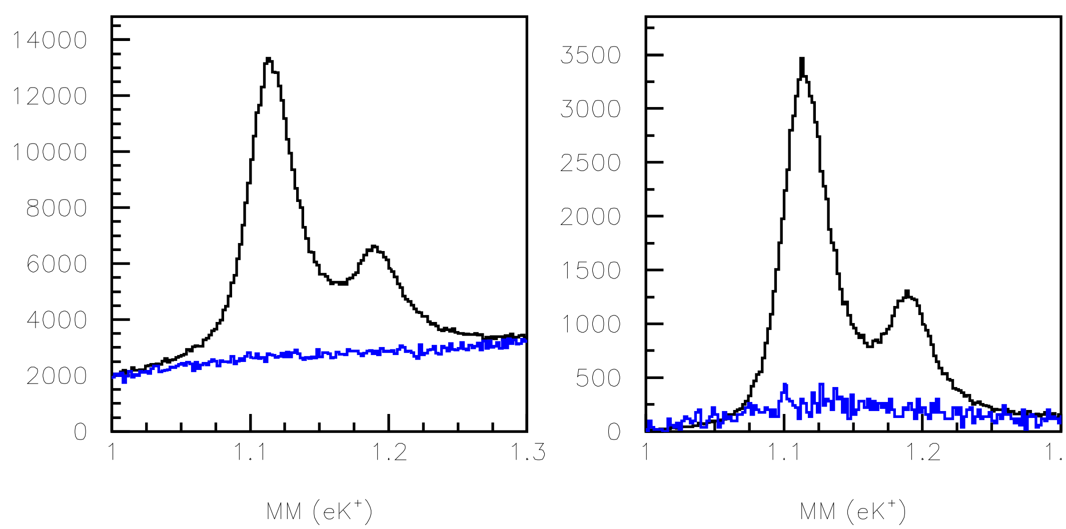

Figure 20: Hyperon missing mass $MM(e'K^+)$ distributions from CLAS e1f data summed over all Q^2, W, and $\cos\theta^*_K$ for the $e'K^+$ topology (left) and the $e'K^+p$ topology (right) with a cut on the $MM^2(e'K^+p)$ distribution on the missing $\pi^-/\pi^-\gamma$ showing the significant reduction in particle misidentification background beneath the hyperons when additional exclusivity cuts are applied to the data. The blue histogram is the particle misidentification background contribution from the reaction $ep \to e'p\pi^+\pi^-$.

As the operating luminosity of CLAS12 will be ten times higher than for CLAS, the expected background levels might be expected to be ∼10 times larger (since the accidental rate scales as the luminosity squared, which is compensation for by the ten times higher event rate). However, the issue of accidentals from misidentified K^+ is mitigated as the particle misidentification levels are reduced. In fact, the particle identification capabilities of CLAS12 are significantly improved compared to those of CLAS as:

- The timing resolution of the CLAS12 FTOF system is about a factor of three better than for the CLAS TOF system [71].
- The HTCC and LTCC systems of CLAS12 are an important component of the hadron identification system that together are 95% $\rightarrow$ 99% efficient for π/K separation for momenta $p > 3$ GeV.

In addition, the backgrounds from particle misidentification in the $MM(e'K^+)$ spectrum are further improved during reconstruction of the final state as:

- The detection of the p from the hyperon decay with a cut on the $MM^2(e'K^+p)$ distribution on the missing π^- (for the $K^+\Lambda$ final state) and the missing $\pi^-\gamma$ (from the $K^+\Sigma^0$ final state) reduces the particle misidentification background by a factor of $\sim$10 as shown in Fig. 20.
- The tracking vertex resolution of CLAS12 in the forward direction ($\theta < 35°$) employing the drift chambers and the micro-megas is roughly a factor of five better than that using the drift chambers of CLAS (2 mm vs. 1 cm). This allows for improved resolution on the detached vertices for the $\Lambda \rightarrow p\pi^-$ decay ($c\tau = 7.89$ cm). This resolution can be expected to allow for cuts to reduce the non-strange background considerably. The development and optimization of this algorithm is planned for later this year.

Further information on accidental rates can be gleaned from our experience with operation of the CLAS detector at a luminosity of $\mathcal{L} = 1 \times 10^{34}$ cm^{-2}s^{-1}. The total hadronic rate in CLAS was measured to be roughly 1 MHz. For a trigger coincidence time window of 100 ns, this gives an accidental rate of 0.1 Hz. For CLAS12 operation at $\mathcal{L} = 1 \times 10^{35}$ cm^{-2}s^{-1} the accidental rate should be at the level of tens of Hz. This rate is not expected to be a limiting factor for exclusive K^+Y final state reconstruction in CLAS12 as it is comparable to the KY production rates in the expected running conditions.

Our nominal approach for the analysis will be to attempt to measure the differential cross sections and separated structure functions from this experiment for the $K^+\Lambda$ and $K^+\Sigma^0$ channels in the topology where only the final state e' and K^+ are detected. This topology results in the highest acceptance for the reactions of interest. All analysis results will be cross-checked from the cross sections measurements determined from the topology that requires detection of the e', K^+, and p in the final state. This final state is, of course, necessary for the analysis to measure the induced and recoil hyperon polarizations. The $MM(e'K^+)$ spectra that could be expected from this experiment are shown requiring the $e'K^+p$ topology in Section 4.4. Although the background levels have been increased by a factor of 10 relative to what has been seen in analysis of data from CLAS (see Fig. 20), this is believed to be a considerable over-estimate of the background levels given that we have not attempted to account for the expected reductions discussed in this section.

Further studies of particle misidentification effects will be studied employing our full CLAS12 GEANT-4 Monte Carlo suite (gemc [72]) later this year after the development of the Monte Carlo and the CLAS12 reconstruction software package [73] are further developed.

4.6 Count Rate Estimates

The K^+Y differential cross section in a given bin of Q^2, W, $\cos\theta_K^*$, and Φ can be written as:

$$\frac{d\sigma}{d\Omega_K^*} = \frac{1}{\mathcal{L}} \cdot \frac{N}{ACC \cdot (\Delta Q^2 \Delta W \Delta \cos\theta_K^* \Delta\Phi)} \cdot \frac{1}{\Gamma_v} \cdot \frac{1}{t_R}, \tag{11}$$

where $\mathcal{L}$ is the beam-target luminosity, N is the number of counts in the bin, ACC is the CLAS12 acceptance for the bin (including all inefficiencies, branching ratios, and dead times), Γ_v is the virtual photon flux factor, and t_R is the run duration.

	E_b=6.6 GeV		E_b=8.8 GeV	
Bin	Q^2 (GeV^2)	W (GeV)	Q^2 (GeV^2)	W (GeV)
1	2.0	1.725	4.0	1.725
2	2.0	1.925	4.0	1.925
3	3.0	1.725	5.0	1.725
4	3.0	1.925	5.0	1.925
5	4.0	1.725	6.0	1.725
6	4.0	1.925	6.0	1.925
7	5.0	1.725	7.0	1.725
8	5.0	1.925	7.0	1.925

Table 2: The eight representative bins in Q^2 and W used for the count rate estimates in this proposal for the 6.6 and 8.8 GeV beam energies.

To determine the expected yields for this experiment, estimates for the $K^+\Lambda$ and $K^+\Sigma^0$ final states were carried out for the eight representative Q^2/W bins for each beam energy as shown in Table 2. These include two values of W (1.725 GeV, 1.925 GeV) and four values of Q^2, 2.0 GeV^2, 3.0 GeV^2, 4.0 GeV^2, 5.0 GeV^2 for E_b=6.6 GeV and 4.0 GeV^2, 5.0 GeV^2, 6.0 GeV^2, 7.0 GeV^2 for E_b=8.8 GeV. In addition, the following assumptions were made:

- $\mathcal{L} = 1 \times 10^{35}$ cm^{-2}s^{-1} - nominal CLAS12 design operating luminosity
- Full torus field ($B = 0.9B_{max}$) with negatively charged particles outbending
- Solenoid at full nominal field
- t_R = 50 days for E_b=6.6 GeV and 50 days for E_b=8.8 GeV
- Γ_v from Eq.(6)
- $d\sigma/d\Omega$ from a $1/Q^2$ extrapolation of the form:

$$d\sigma/d\Omega = \mathcal{C}_1 \cdot \left(\mathcal{C}_2 + Q^2\right)^{-1} \tag{12}$$

  to the electroproduction cross sections in each $\cos\theta_K^*$ bin from Ref. [39].
- Binning:

- $\Delta Q^2 = 1.0$ GeV^2
- $\Delta W = 50$ MeV,
- $\Delta \cos\theta^*_K$ 10 bins:

  [-0.90,-0.65], [-0.65,-0.40], [-0.40,-0.20], [-0.20,0.00], [0.00,0.20], [0.20,0.40], [0.40,0.60], [0.60,0.75], [0.75,0.90], [0.90,1.00]
- $\Delta\Phi$: 8 bins 45°-wide [-180°,180°]

  ($\cos\theta^*_K$ and Φ binning chosen to match e1f analysis)

- *ACC* from fastMC with a reasonably realistic event distribution for the event generator.

The acceptances in each kinematic bin were determined from the ratio of reconstructed to generated events in each bin. The acceptances determined for the $K^+\Lambda$ final state for the $e'K^+$ and $e'K^+p$ topologies are shown in Fig. 21 and Fig. 22, respectively, for the eight bins of Table 2 averaged over Φ. The acceptances for the $K^+\Sigma^0$ final state are comparable. The studies show typical Φ-averaged $e'K^+$ topology acceptances of 50% and typical Φ-averaged $e'K^+p$ topology acceptances of 25%, relatively independent of kinematics.

Figures 23 and 24 show the expected yields determined using Eq.(11) for the $K^+\Lambda$ final state for both the $e'K^+$ and $e'K^+p$ topologies for E_b=6.6 GeV and 8.8 GeV, respectively. Figs. 25 and 26 show the corresponding yields expected for the $K^+\Sigma^0$ final state. Also shown in these figures are the measured yields from the e1f analysis at Q^2=1.8 GeV^2 (from Ref. [39]) for the $e'K^+$ topology, which we might consider as a reasonable measure of the required statistics for a viable experiment. A comparison of the expected yields from this proposed experiment at E_b=6.6 GeV and 8.8 GeV and the existing CLAS data from Refs. [39] shows an increase of a factor of 10 to 100 for the $e'K^+$ topology in the range from Q^2=2 GeV^2 to 4 GeV^2. For Q^2 in the range from 4 GeV^2 to 7 GeV^2, the expected statistics even in the $e'K^+p$ topology are comparable to the statistics from our already published CLAS data at Q^2=1.8 GeV^2 in the $e'K^+$ topology. These statistics are judged to be sufficient to successfully complete both the Stage 1 and Stage 2 analysis programs as described in Sections 4.2 and 4.3, respectively.

Note the $1/Q^2$ extrapolation was found to be the most reasonable to fit the existing CLAS data in the range of Q^2 up to 4 GeV^2. However, the expected yields were also studied using a $1/Q^4$ extrapolation of the cross sections in Ref. [39] as:

$$d\sigma/d\Omega = \mathcal{C}_1 \cdot \left(\mathcal{C}_2 + Q^2\right)^{-2}, \tag{13}$$

and the corresponding expected yields were reduced by a factor of two. We would also like to make clear that these count rate estimates will be repeated later this year with the full CLAS12 GEANT-4 gemc Monte Carlo [72] with the full CLAS12 event reconstruction package [73]. Preliminary comparisons of the CLAS12 response using the fastMC code suite and the CLAS12 gemc code suite have shown to yield reasonably good correspondence.

5 Summary and Beam Time Request

The studies of the electromagnetic transition amplitudes between the nucleon ground and excited states over a wide range of Q^2 elucidate the relevant degrees of freedom in the N^*

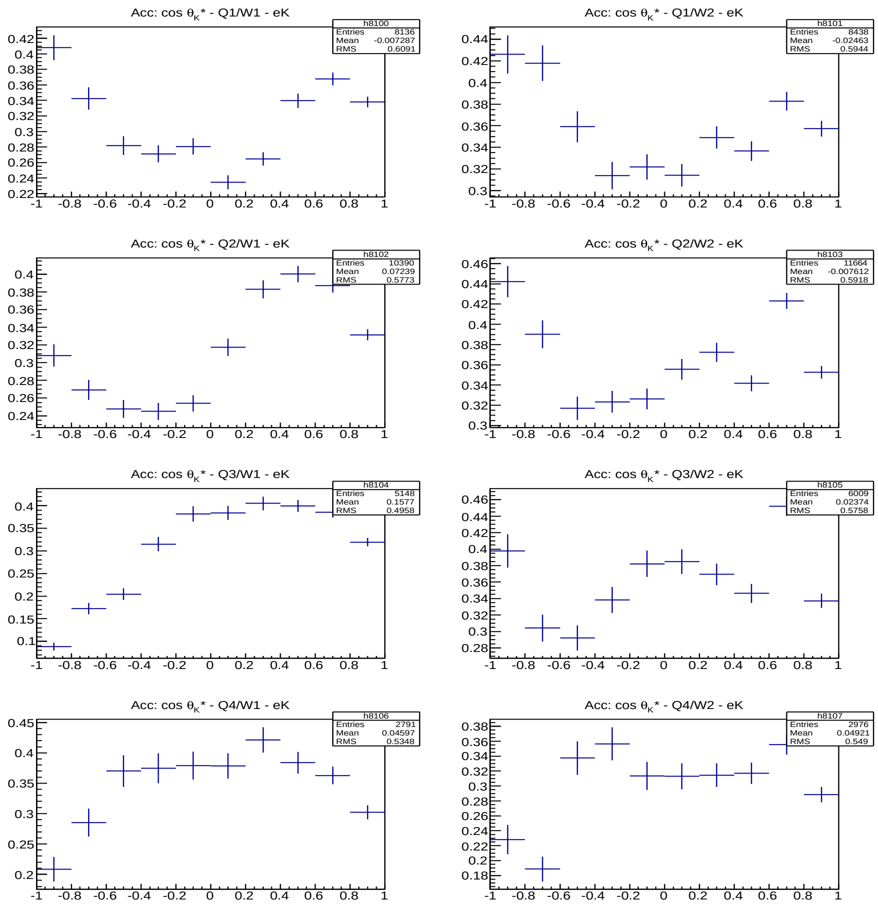

Figure 21: Acceptance functions determined from the Monte Carlo simulations for E_b=6.6 GeV with the torus set at $B = 0.9B_{max}$ for negatively charged particles outbending as a function of $\cos\theta^*_K$ averaged over Φ for the $K^+\Lambda$ final state for the $e'K^+$ topology for W=1.725 GeV (left) and W=1.925 GeV (right) for each of the four Q^2 bins listed in Table 2, Q^2=2.0 GeV^2 (top row), 3.0 GeV^2 (second row), 4.0 GeV^2 (third row), and 5.0 GeV^2 (bottom row). These acceptances were determined with a thrown event sample of 10M events and yield statistical uncertainties on the acceptance of a few percent.

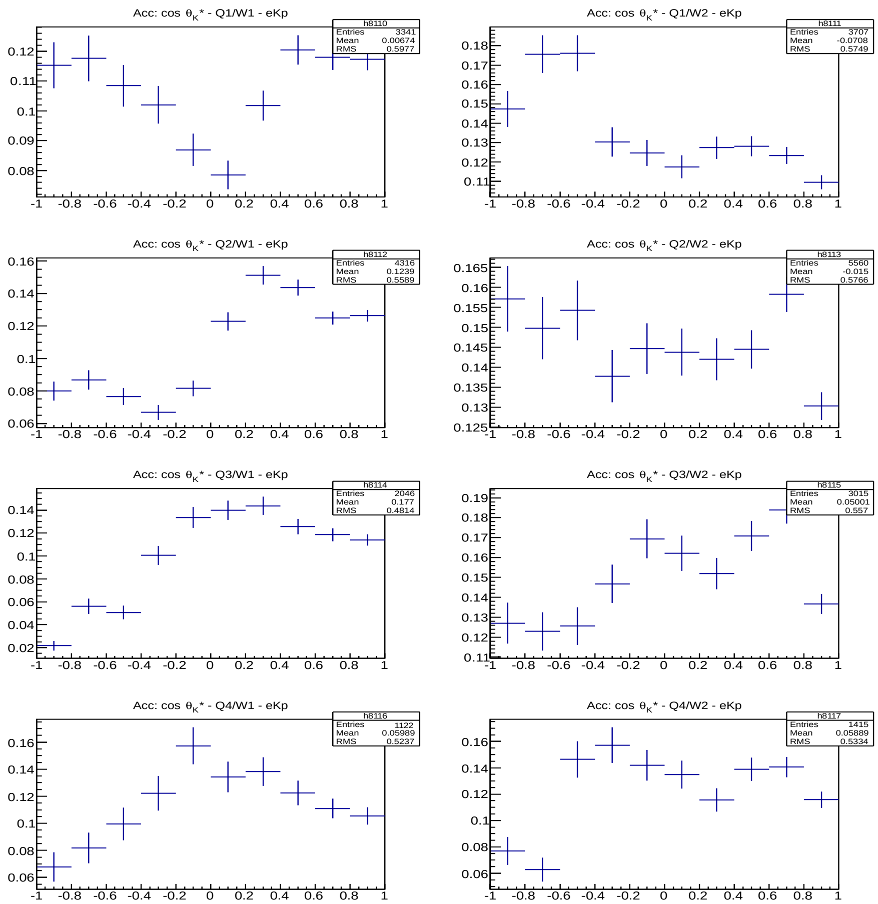

Figure 22: Acceptance functions determined from the Monte Carlo simulations for E_b=6.6 GeV with the torus set at $B = 0.9B_{max}$ for negatively charged particles outbending as a function of $\cos\theta^*_K$ averaged over Φ for the $K^+\Lambda$ final state for the $e'K^+p$ topology for W=1.725 GeV (left) and W=1.925 GeV (right) for each of the four Q^2 bins listed in Table 2, Q^2=2.0 GeV^2 (top row), 3.0 GeV^2 (second row), 4.0 GeV^2 (third row), and 5.0 GeV^2 (bottom row). These acceptances were determined with a thrown event sample of 10M events and yield statistical uncertainties on the acceptance of a few percent.

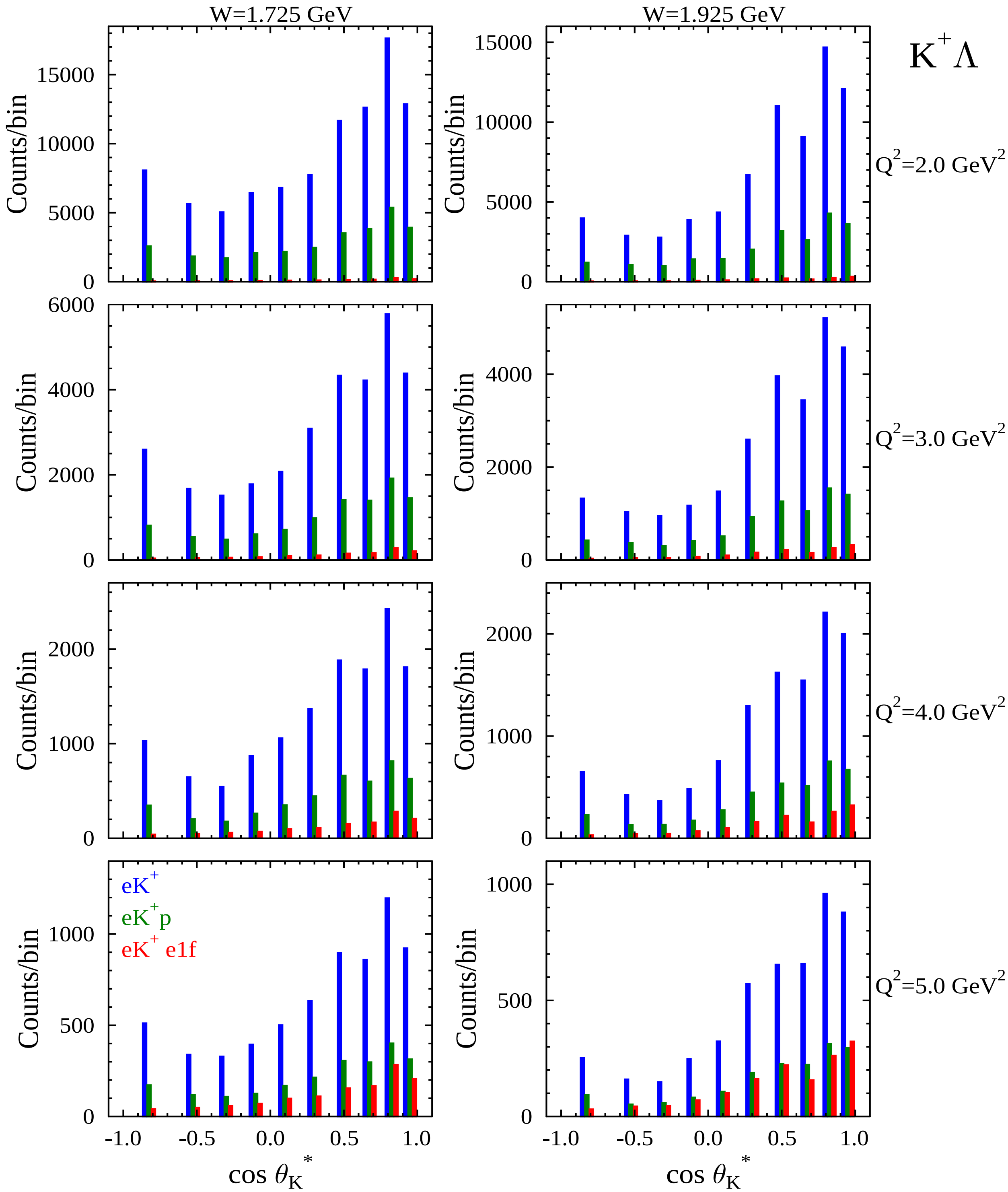

Figure 23: Expected counts in the eight bins of Table 2 at Q^2=2.0 GeV^2, 3.0 GeV^2, 4.0 GeV^2, and 5.0 GeV^2 for the $K^+\Lambda$ final state for E_b=6.6 GeV with the torus set at $B = 0.9B_{max}$ for negatively charged particles outbending at two representative values of W=1.725 GeV, 1.925 GeV averaged over Φ for a 50 day run at a luminosity of 1×10^{35} cm^{-2}s^{-1} for the $e'K^+$ topology (blue bars) and $e'K^+p$ topology (green bars) compared to the $e'K^+$ yields from the e1f experiment at Q^2=1.8 GeV^2 (red bars) of Ref. [39].

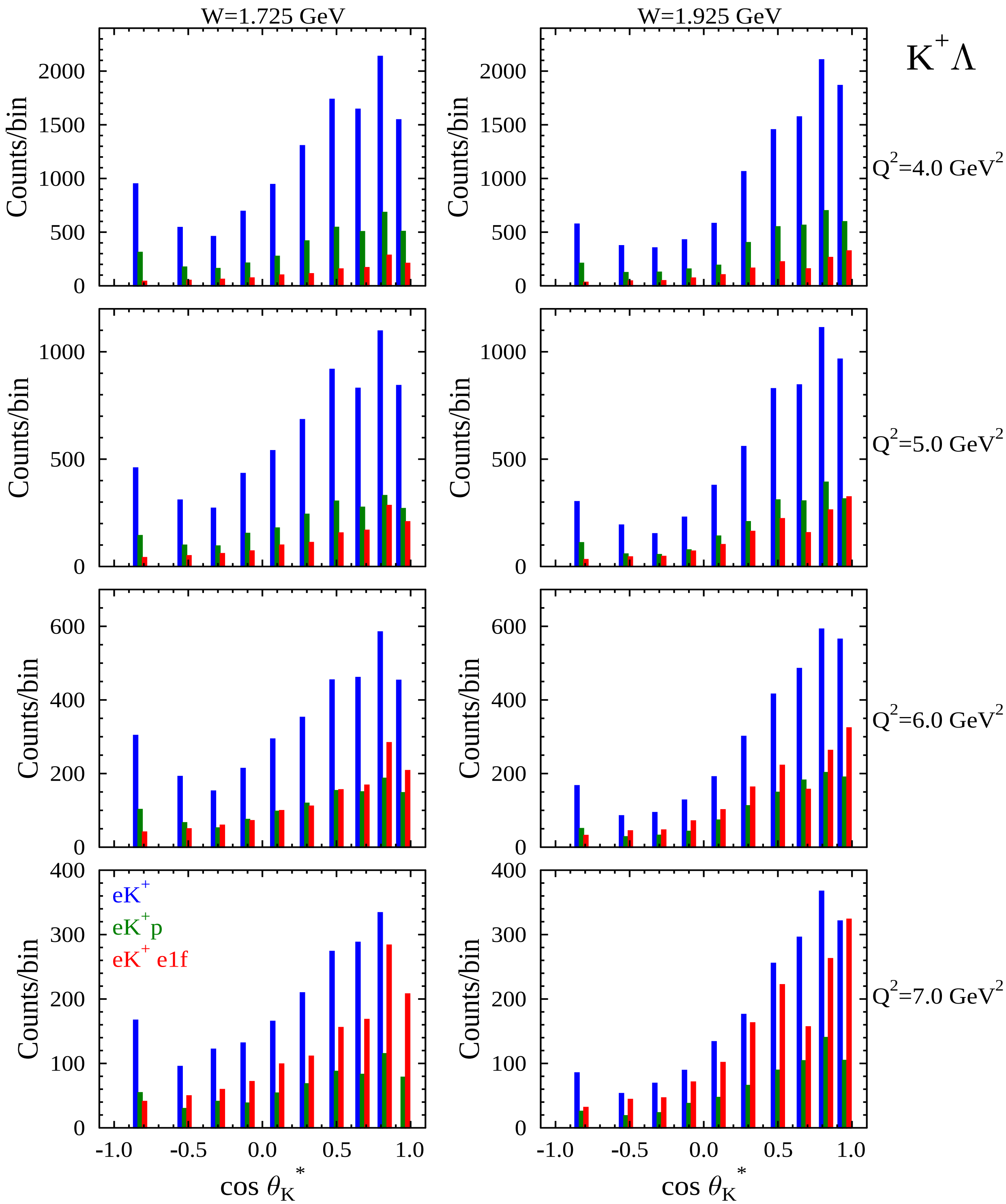

Figure 24: Expected counts in the eight bins of Table 2 at Q^2=4.0 GeV^2, 5.0 GeV^2, 6.0 GeV^2, and 7.0 GeV^2 for the $K^+\Lambda$ final state for E_b=8.8 GeV with the torus set at $B = 0.9B_{max}$ for negatively charged particles outbending at two representative values of W=1.725 GeV, 1.925 GeV averaged over Φ for a 50 day run at a luminosity of 1×10^{35} cm^{-2}s^{-1} for the $e'K^+$ topology (blue bars) and $e'K^+p$ topology (green bars) compared to the $e'K^+$ yields from the e1f experiment at Q^2=1.8 GeV^2 (red bars) of Ref. [39].

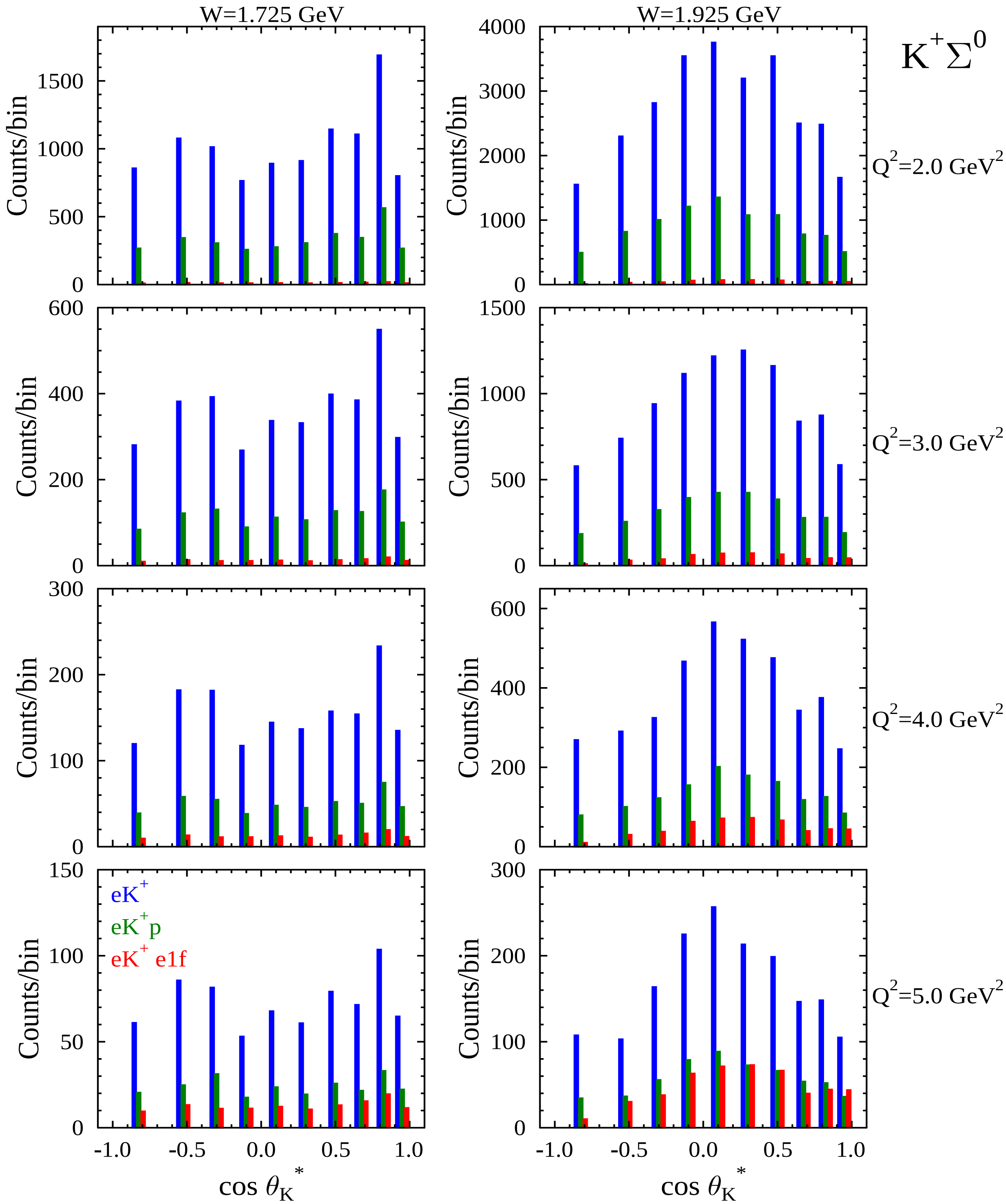

Figure 25: Expected counts in the eight bins of Table 2 at Q^2=2.0 GeV^2, 3.0 GeV^2, 4.0 GeV^2, and 5.0 GeV^2 for the $K^+\Sigma^0$ final state for E_b=6.6 GeV with the torus set at $B = 0.9B_{max}$ for negatively charged particles outbending at two representative values of W=1.725 GeV, 1.925 GeV averaged over Φ for a 50 day run at a luminosity of 1×10^{35} cm^{-2}s^{-1} for the $e'K^+$ topology (blue bars) and $e'K^+p$ topology (green bars) compared to the $e'K^+$ yields from the e1f experiment at Q^2=1.8 GeV^2 (red bars) of Ref. [39].

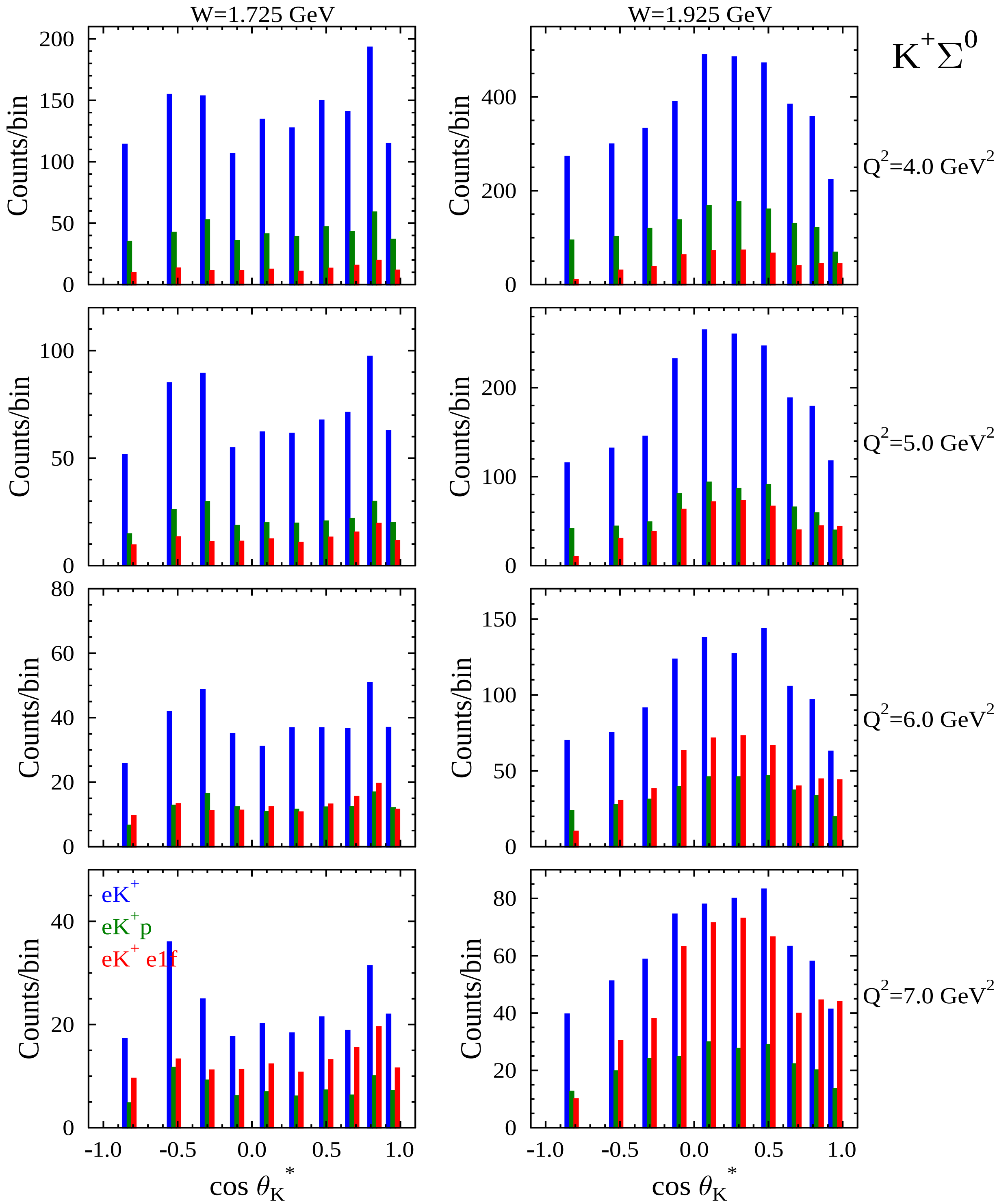

Figure 26: Expected counts in the eight bins of Table 2 at Q^2=4.0 GeV^2, 5.0 GeV^2, 6.0 GeV^2, and 7.0 GeV^2 for the $K^+\Sigma^0$ final state for E_b=8.8 GeV with the torus set at $B = 0.9B_{max}$ for negatively charged particles outbending at two representative values of W=1.725 GeV, 1.925 GeV averaged over Φ for a 50 day run at a luminosity of 1×10^{35} cm^{-2}s^{-1} for the $e'K^+$ topology (blue bars) and $e'K^+p$ topology (green bars) compared to the $e'K^+$ yields from the e1f experiment at Q^2=1.8 GeV^2 (red bars) of Ref. [39].

structure at different distance scales and will allow for a better understanding of the non-perturbative strong interaction that governs the formation of the N^* states. With the JLab 12-GeV upgrade and the new CLAS12 detector, a unique opportunity is available to probe the structure of nucleon resonances over a broad range of Q^2.

In recent years the CLAS Collaboration has succeeded in determining the Q^2 evolution of baryon resonance electrocoupling amplitudes from unpolarized $N\pi$ and $N\pi\pi$ electroproduction data. These studies make clear that the independent analysis of multiple final states in the same kinematic domain is essential to minimize the systematics of the measurements and to have confidence in the extracted electrocoupling parameters. In terms of pionic coupling, most high-lying N^* states preferentially decay through the $N\pi\pi$ channel instead of the $N\pi$ channel. Thus data from the KY channels is critical to provide an independent extraction of the electrocoupling amplitudes for the high-lying N^* states against those determined from the analysis of the $N\pi\pi$ channel.

The CLAS12 N^* program already consists of two approved experiments. E12-09-003 [9] will focus on studies of N^* states from the single non-strange meson and $N\pi\pi$ channels. E12-06-108A [10] will focus specifically on the study of N^* states from the strangeness channels with a focus on the exclusive $K^+\Lambda$ and $K^+\Sigma^0$ reactions. Both E12-09-003 and E12-06-108A are part of the first physics running period with CLAS12 that will employ a longitudinally polarized 11 GeV electron beam. These two experiments seek to extract the electrocouplings of all prominent N^* and Δ^* excited states spanning the full nucleon resonance region up to W=3 GeV in the almost unexplored region of Q^2 from 5 GeV^2 to 12 GeV^2.

This proposal extends the physics reach of the existing CLAS12 N^* program and specifically E12-06-108A through measurements of the $K^+\Lambda$ and $K^+\Sigma^0$ final states using longitudinally polarized electron beams of energies E_b=6.6 GeV and 8.8 GeV. The Q^2 coverage from 2 GeV^2 to 7 GeV^2 covered by the data from this proposal makes this extension of the N^* program the most suitable for the exploration of the emergence of the outer meson-baryon cloud in the structure of N^* states from the regime of quark-gluon confinement. These data will allow for precision measurements of cross sections and separated structure functions σ_U, σ_{LT}, σ_{TT}, and $\sigma_{LT'}$, as well as the induced and beam-recoil transferred hyperon polarizations in the Q^2 range from 2 GeV^2 to 7 GeV^2.

The count rate estimates have been carried out assuming 50 days of data taking at both 6.6 GeV and 8.8 GeV beam energies. The K^+Y yields as computed from the CLAS12 fastMC simulation reconstructing the final state by detection of the e' and K^+ are expected to be nearly two orders of magnitude higher compared to those from the measurements already carried out using CLAS for Q^2 up to 4 GeV^2. In the Q^2 range from 4 GeV^2 to 7 GeV^2, the computed yields are expected to be a factor of $\sim$3 larger than what was acquired with the CLAS dataset at Q^2=1.8 GeV^2.

For the foreseeable future, CLAS12 will be the only facility in the world capable of investigating the spectrum and the structure of excited nucleon states at distance scales from low to high Q^2, encompassing the regime where low-energy meson-baryon degrees of freedom dominate to the regime where the quark degrees of freedom are expected to dominate. The extraction of the $\gamma_v NN^*$ transition amplitudes for the prominent N^* and Δ^* states from the comprehensive data based on this experiment, together with those provided by the already approved N^* experiments of the 12 GeV program, will allow for the opportunity to better understand how the strong interaction of dressed quarks gives rise to the spectrum and structure of excited nucleon states, and how these states emerge from QCD.

This proposal is designed to be fully compatible with the new CLAS12 run group featuring the experiment to study hybrid baryons running with 100 days total beam time at electron beam energies of 6.6 GeV and 8.8 GeV upon an unpolarized liquid-hydrogen target at a beam-target luminosity of $\mathcal{L} = 1 \times 10^{35}$ cm^{-2}s^{-1} with the maximum torus current operated with negatively charged particles outbending. We request that the JLab PAC approve this experiment as part of the Jefferson Laboratory physics program in Hall B and recognize its importance as an extension to the existing CLAS12 N^* program at high Q^2. This proposal has been reviewed internally within the CLAS Collaboration and has been fully endorsed by the CLAS Collaboration.

The participation of the different research groups that are a part of this proposal has been fully detailed in the proposal for E12-06-108A [74]. The data collected as part of this lower energy running will be considered another aspect of the existing effort.

References

[1] N. Isgur and G. Karl, Phys. Rev. D **19**, 2653 (1979).

[2] S. Capstick and N. Isgur, Phys. Rev. D **34**, 2809 (1986).

[3] I.G. Aznauryan and V.D. Burkert, Prog. Part. Nucl. Phys. **67**, 1 (2012).

[4] J. Segovia *et al.*, Phys. Rev. Lett. **115**, 171801 (2015).

[5] I.C. Cloët and C.D. Roberts, Prog. Part. Nucl. Phys. **77**, 1 (2014).

[6] I.V. Anikin *et al.*, Phys. Rev. D **92**, 014018 (2015).

[7] H. Kamano, S.X. Nakamura, T.-S.H. Lee, and T. Sato, Phys. Rev. C **88**, 035201 (2013).

[8] I.G. Aznauryan *et al.*, Int. J. Mod. Phys. **E22**, 1330015 (2013).

[9] JLab Experiment E12-09-003, spokespersons: V.D. Burkert, P. Cole, R. Gothe, K. Joo, V. Mokeev, P. Stoler

[10] JLab Experiment E12-06-108A, spokespersons: D.S. Carman, R. Gothe, V. Mokeev

[11] C.D. Roberts, arXiv:1509.02925, (2015).

[12] C.D. Roberts, J. Phys. Conf. Ser.**630**, 012051 (2015).

[13] U. Löhring, B.C. Metsch, and H.R. Petry, Eur. Phys. J. A **10**, 395 (2001).

[14] J. Beringer *et al.* (PDG), Phys. Rev. D **86**, 010001 (2012).

[15] B. Julia-Diaz, D.O. Riska, and F. Coester, Phys. Rev. C **79**, 035212 (2004).

[16] I.G. Aznauryan, Phys. Rev. C **76**, 025212 (2007).

[17] I.G. Aznauryan and V.D. Burkert, Phys. Rev. C **85**, 055202 (2012).

[18] I.G. Aznauryan and V.D. Burkert, arXiv:1603.06692, (2016).

[19] C.S. An *et al.*, Phys. Rev. C **74** 055205 (2006).

[20] M. Aiello, M.M. Giannini, and E. Santopinto, J. Phys. G **24**, 753 (1998)

[21] M. De Sanctis *et al.*, Phys. Rev. C **76**, 062202 (2007).

[22] M. Bhagwat and P. Tandy, AIP Conf. Proc. **842**, 225 (2006).

[23] C.D. Roberts, Prog. Part. Nucl. Phys. **61**, 55 (2008).

[24] C. Chen *et al.*, Few Body Syst. **53**, 293 (2012).

[25] V. Pascalutsa, M. Vanderhaeghen, and S.N. Yang, Phys. Rept. **437**, 125 (2007).

[26] M.V. Polyakov and K.M. Semenov-Tian-Shansky, Eur. Phys. J. A **40**, 181 (2009).

[27] USQCD Collaboration, http://www.usqcd.org/collaboration.html.

[28] Jefferson Laboratory Joint Physics Analysis Center, https://jpac.jlab.org/.

[29] B.A. Mecking *et al.*, Nucl. Inst. and Meth. A **503**, 513 (2003).

[30] V.I. Mokeev and I.G. Aznauryan, Int. J. Mod. Phys. Conf. Ser. **26**, 1460080 (2014).

[31] V.I. Mokeev. Presentation at the ECT* Workshop, *Nucleon Resonances: From Photoproduction to High Photon Virtualities*, (2015).

[32] V.I. Mokeev *et al.*, Phys. Rev. C **93**, 025206 (2016).

[33] I.G. Aznauryan *et al. (CLAS Collaboration)*, Phys. Rev. C **80**, 055203 (2009).

[34] K. Park *et al. (CLAS Collaboration)*, Phys. Rev. C **91**, 045203 (2015).

[35] I.G. Aznauryan and V.D. Burkert, Phys. Rev. C **92**, 015203 (2015).

[36] B.A. Raue and D.S. Carman, Phys. Rev. C **71**, 065209 (2005).

[37] P. Ambrozewicz *et al. (CLAS Collaboration)*, Phys. Rev. C **75**, 045203 (2007).

[38] R. Nasseripour *et al. (CLAS Collaboration)*, Phys. Rev. C **77**, 065208 (2008).

[39] D.S. Carman *et al. (CLAS Collaboration)*, Phys. Rev. C **87**, 025204 (2013).

[40] M. Gabrielyan *et al. (CLAS Collaboration)*, Phys. Rev. C **90**, 035202 (2014).

[41] D.S. Carman *et al. (CLAS Collaboration)*, Phys. Rev. Lett. **90**, 131804 (2003).

[42] D.S. Carman *et al. (CLAS Collaboration)*, Phys. Rev. C **79**, 065205 (2009).

[43] CLAS physics database, http://clasweb.jlab.org/physicsdb.

[44] O. Maxwell, Phys. Rev. C **85**, 034611 (2012).

[45] L. De Cruz *et al.*, Phys. Rev. C **86**, 015212 (2012).

[46] T. Corthals *et al.*, Phys. Lett. B **656**, 186 (2007).

[47] A.V. Anisovich *et al.*, Eur. Phys. J A **48**, 15 (2012).

[48] E. Klempt and R. Workman, https://pdg.web.cern.ch/pdg/2012/reviews/rpp2012-rev-n-delta-resonances.pdf.

[49] V.A. Nikonov *et al.*, Phys. Lett. B **662**, 245 (2008).

[50] B. Julia-Diaz *et al.*, Nucl. Phys. A **755**, 463 (2005); B. Julia-Diaz *et al.*, Phys. Rev. C **73**, 055204 (2006).

[51] T. Mart and A. Sulaksono, Phys.Rev. C **74**, 055203 (2006).

[52] A.V. Anisovich *et al.*, Eur. Phys. J. A **48**, 88 (2012).

[53] P.O. Bowman *et al.*, Phys. Rev. D **71**, 054507 (2005).

[54] I.C. Cloët, C.D. Roberts, and A.W. Thomas, Phys. Rev. Lett **111**, 101803 (2013).

[55] White Paper of the JLab Workshop, *"Electromagnetic N-N* Transition Form Factors"*, Newport News, VA, USA, October 13-15, 2008.

[56] L.L. Frankfurt *et al.*, Phys. Rev. Lett. **84**, 2589 (2000).

[57] K. Goeke, M.V. Polyakov, and M. Vanderhaeghen, Prog. Part. Nucl. Phys. **47**, 401 (2001).

[58] I.V. Anikin, V.M. Braun, N. Offen, Phys. Rev. D **92**, 014018 (2015).

[59] See CLAS12 web page at http://www.jlab.org/Hall-B/clas12-web.

[60] G. Knöchlein, D. Drechsel, L. Tiator, Z. Phys. **A 352**, 327 (1995).

[61] S. Boffi, C. Giusti, and F.D. Pacati, Phys. Rep. **226**, 1 (1993); S. Boffi, C. Giusti, and F.D. Pacati, Nucl. Phys. A **435**, 697 (1985).

[62] C.W. Akerlof *et al.*, Phys. Rev. **163**, 1482 (1967).

[63] A. Afanasev, I. Akushevich, V. Burkert, and K. Joo, Phys. Rev. D **66**, 074004 (2002).

[64] B.E. Bonner *et al.*, Phys. Rev. D **38**, 729 (1988).

[65] L. Tiator *et al.*, Eur. Phys. J. ST **198**, 141 (2011).

[66] I. Aznauryan, Phys. Rev. C **67**, 015209 (2003).

[67] V. Mokeev *et al. (CLAS Collaboration)*, Phys. Rev. C **86**, 035203 (2012).

[68] V.I. Mokeev *et al.*, Phys. Rev. C **80**, 045212 (2009).

[69] M. Döring, Int. J. Mod. Phys. Conf. Ser. **26**, 1460054 (2014).

[70] JPARC Experiment P45, *3-Body Hadronic Reactions for New Aspects of Baryon Spectroscopy*, K.H. Hicks and H. Sako spokesperson.

[71] D.S. Carman, FTOF Project Close-out Slides, https://www.jlab.org/Hall-B/ftof/ftof-closeout.pdf

[72] GEMC Documentation,
see https://gemc.jlab.org/gemc/Documentation/Documentation.html

[73] CLAS12 Software Development,
see http://clasweb.jlab.org/clas12offline/docs/software/html/

[74] E12-06-108 proposal, see https://userweb.jlab.org/ carman/ky12/ky12-prop.pdf (Section 6).